Fig.S1

FACS analyis after release from synchronization

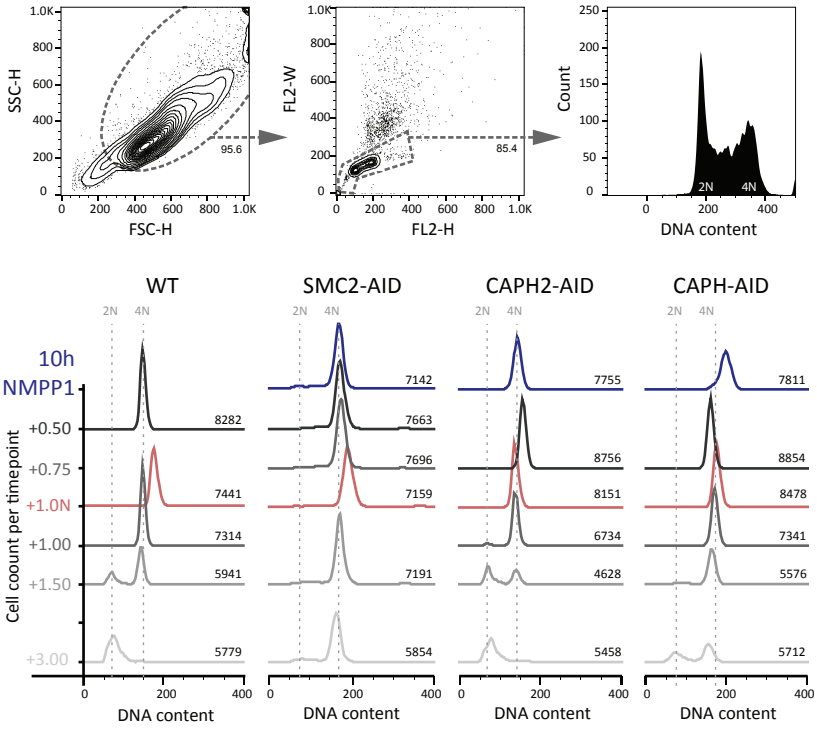

Fig.S2

NEBD visualized by Lamin staining

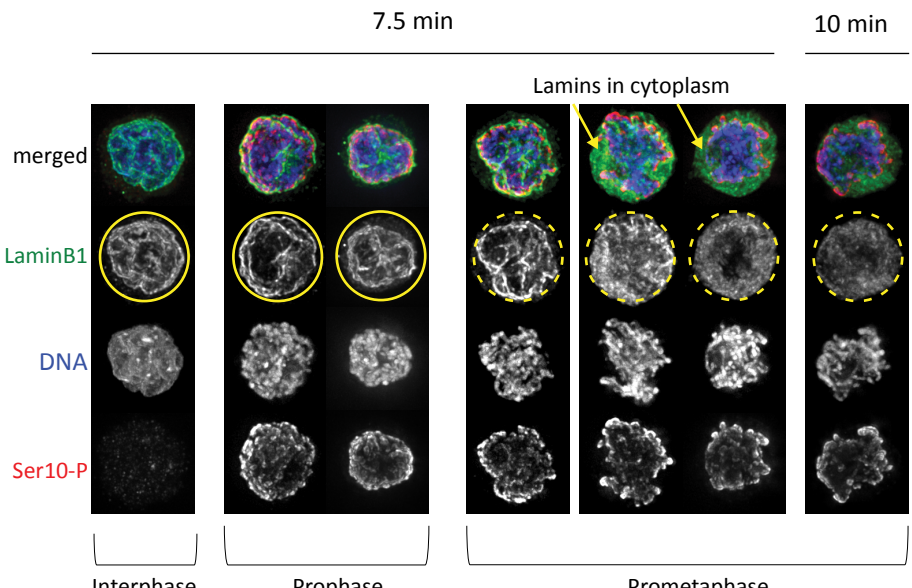

Fig.S3

WT

A

Images corresponding to samples for condensin ChEP data

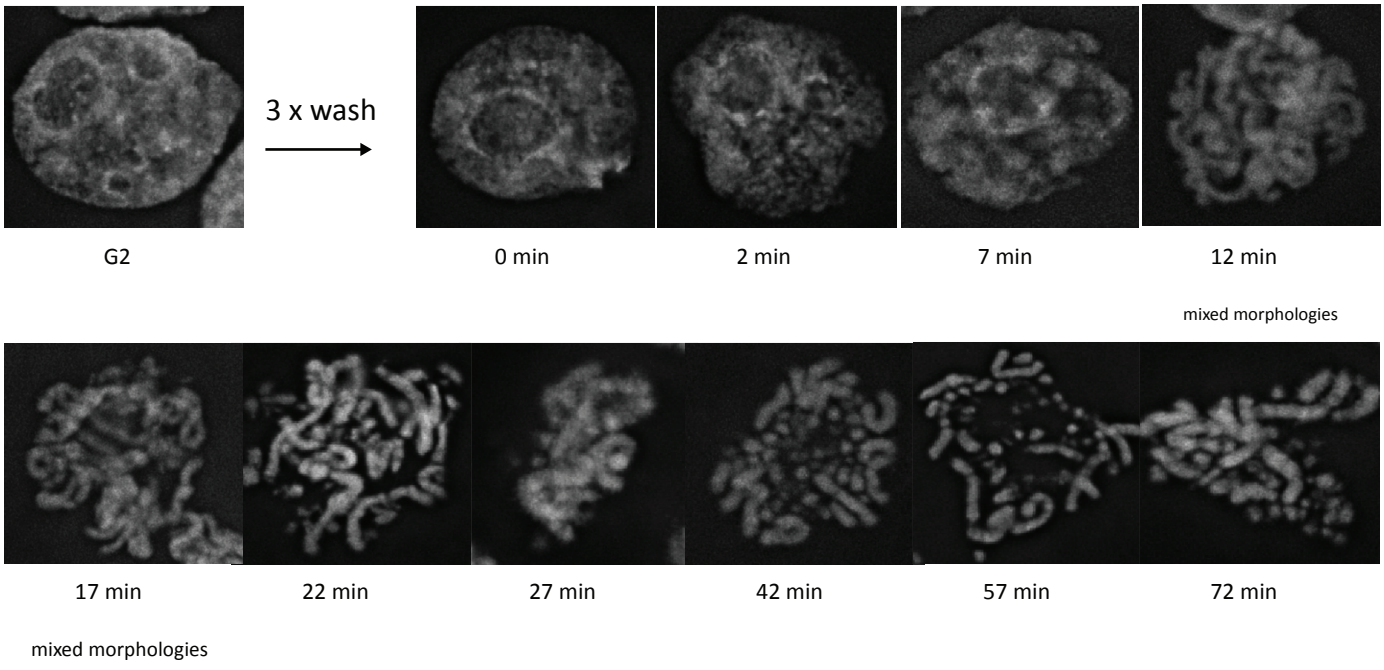

B WT

C CAPH-AID

D Cohesin/CTCF

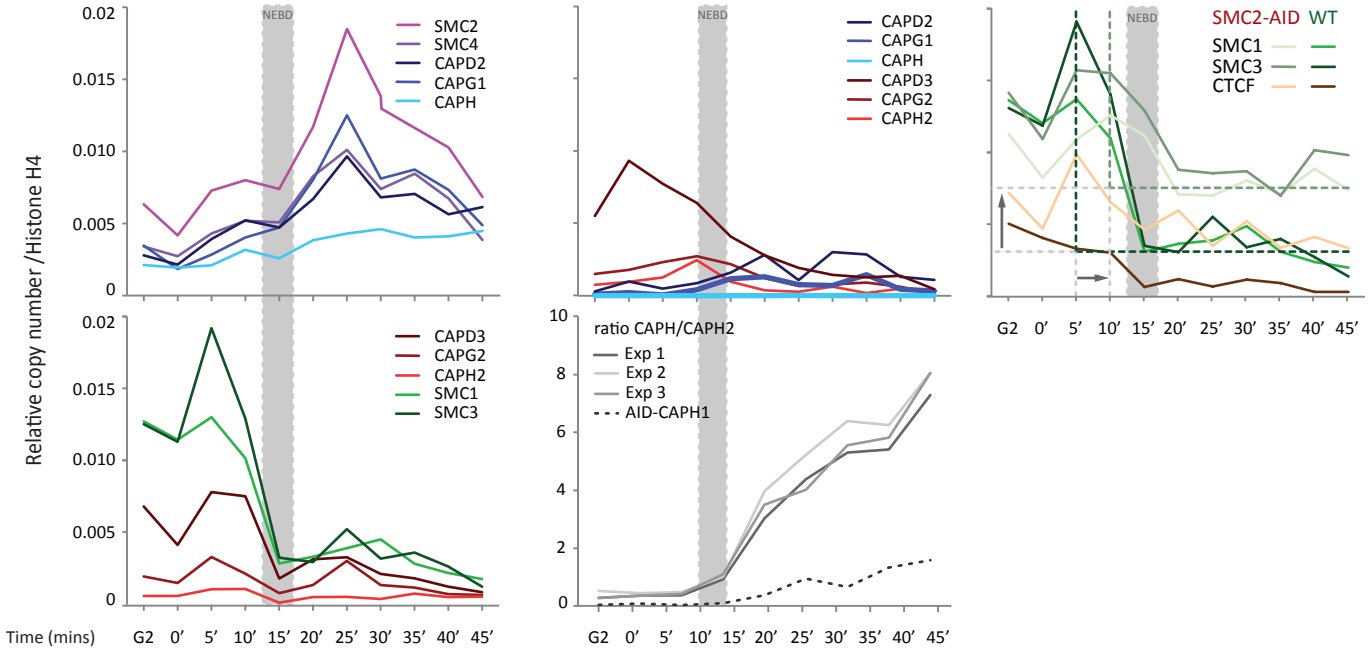

Fig.S4

A Insulation analysis at varying length scales

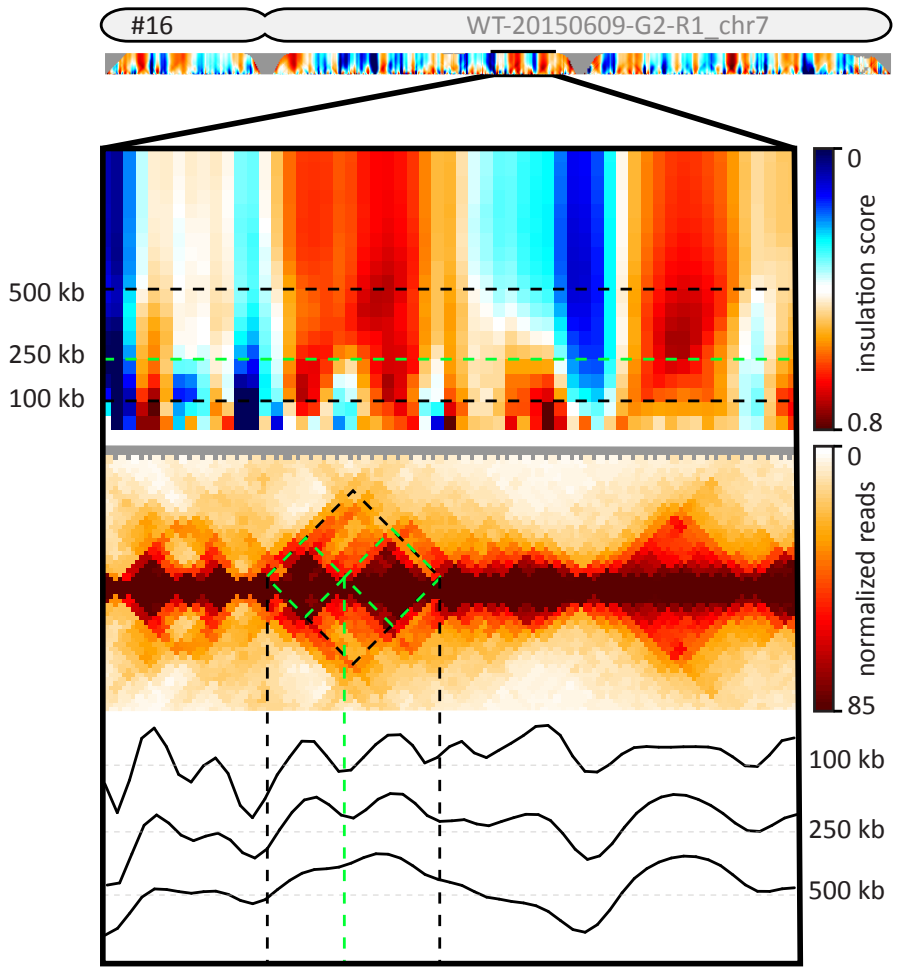

B Insulation score variance

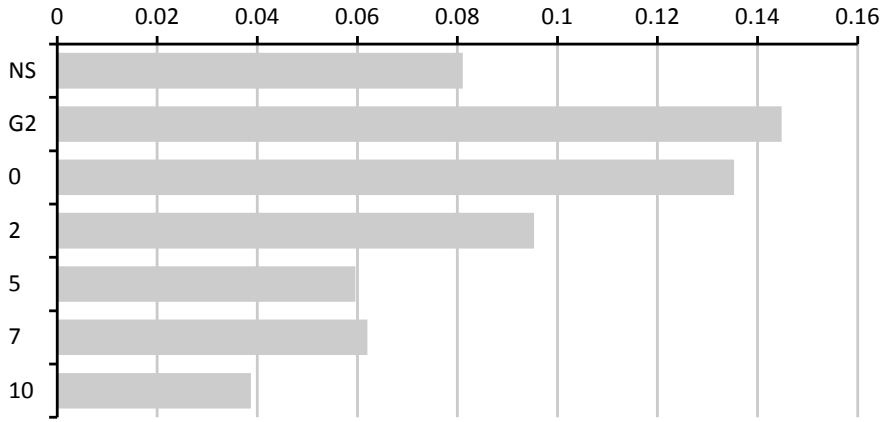

Fig.S5

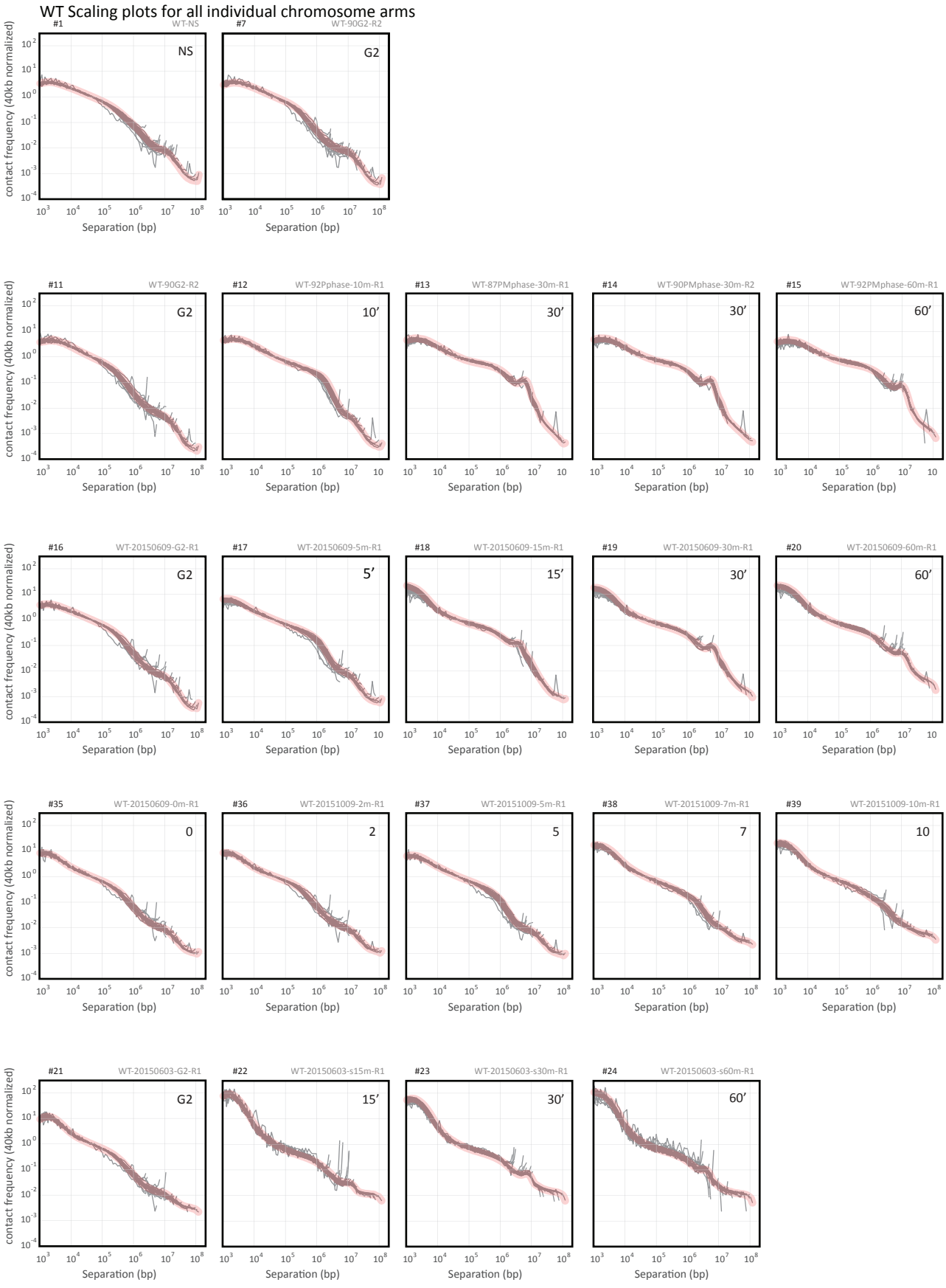
WT Scaling plots for all individual chromosome arms
#1 WT-NS
NS
#7 WT-90G2-R2
G2
#11 WT-90G2-R2
G2
#12 WT-92Pphase-10m-R1
10′
#13 WT-87PMphase-30m-R1
30′
#14 WT-90PMphase-30m-R2
30′
#15 WT-92PMphase-60m-R1
60′
#16 WT-20150609-G2-R1
G2
#17 WT-20150609-5m-R1
5′
#18 WT-20150609-15m-R1
15′
#19 WT-20150609-30m-R1
30′
#20 WT-20150609-60m-R1
60′
#35 WT-20150609-0m-R1
0
#36 WT-20151009-2m-R1
2
#37 WT-20151009-5m-R1
5
#38 WT-20151009-7m-R1
7
#39 WT-20151009-10m-R1
10
#21 WT-20150603-G2-R1
G2
#22 WT-20150603-s15m-R1
15′
#23 WT-20150603-s30m-R1
30′
#24 WT-20150603-s60m-R1
60′
contact frequency (40kb normalized)
Separation (bp)

Fig.S6

Heatmaps from all individual libraries for WT chromosome 7

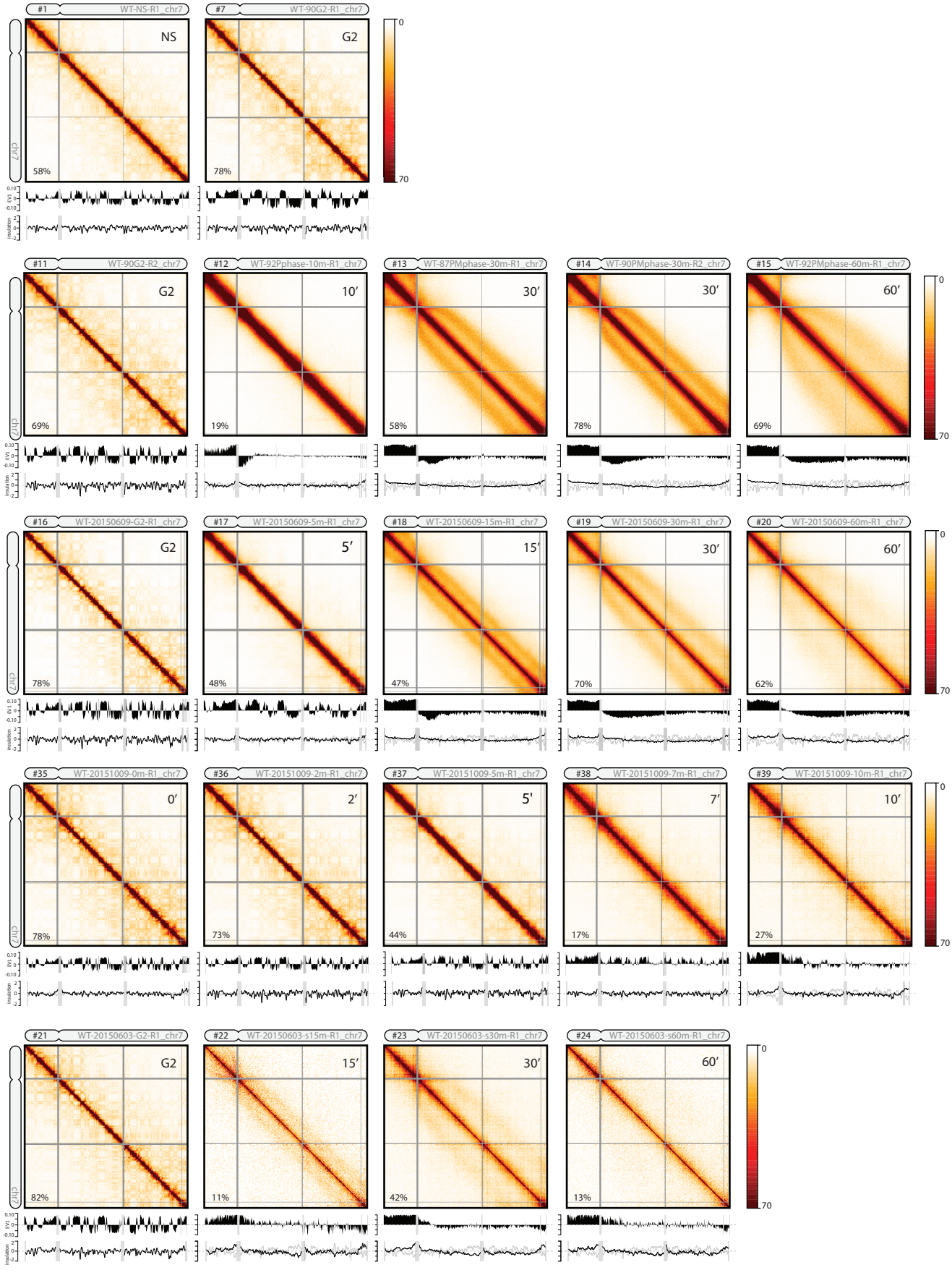

Fig.S7

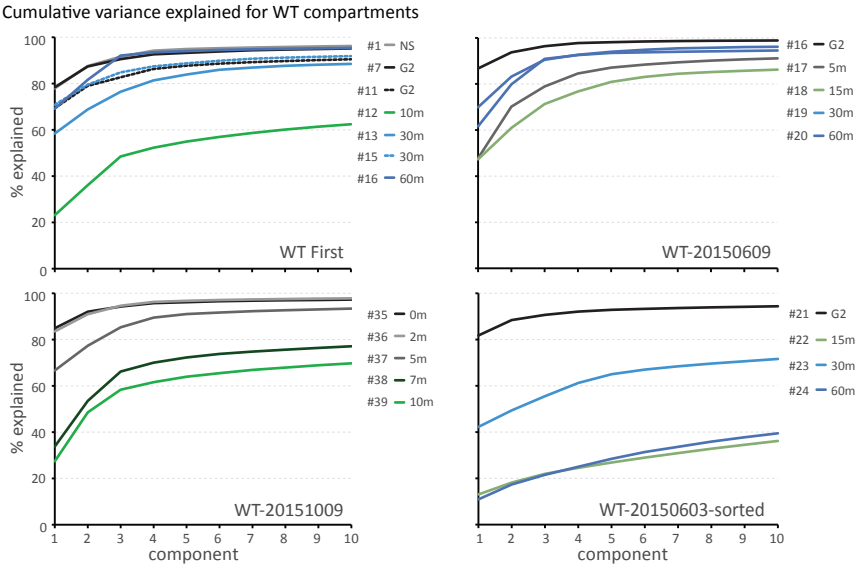
Cumulative variance explained for WT compartments
% explained
component
WT First
#1 NS
#7 G2
#11 G2
#12 10m
#13 30m
#15 30m
#16 60m
WT-20150609
#16 G2
#17 5m
#18 15m
#19 30m
#20 60m
WT-20151009
#35 0m
#36 2m
#37 5m
#38 7m
#39 10m
WT-20150603-sorted
#21 G2
#22 15m
#23 30m
#24 60m

Fig.S8

Saddle plots for all individual chromosome arms from WT

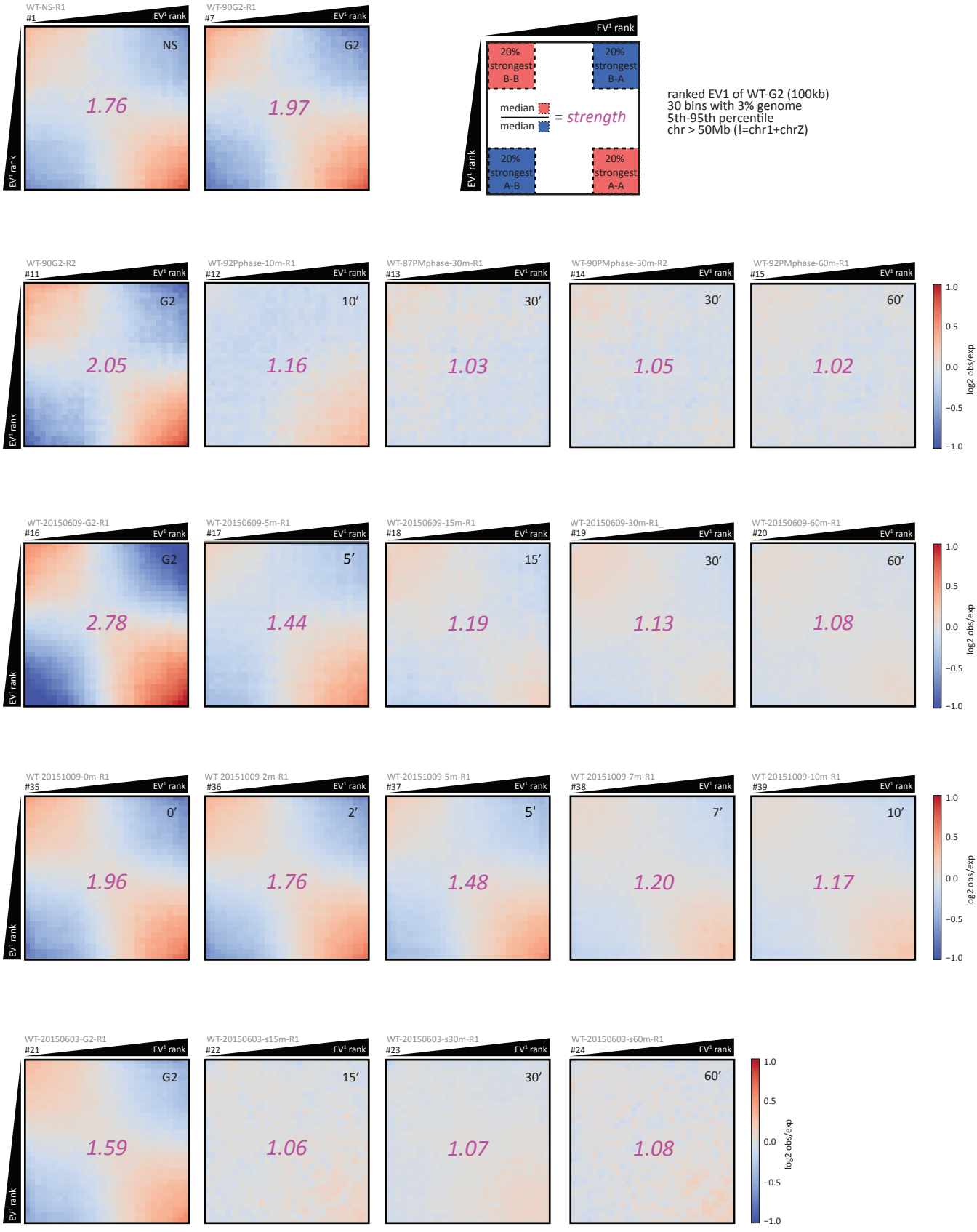

Fig.S9

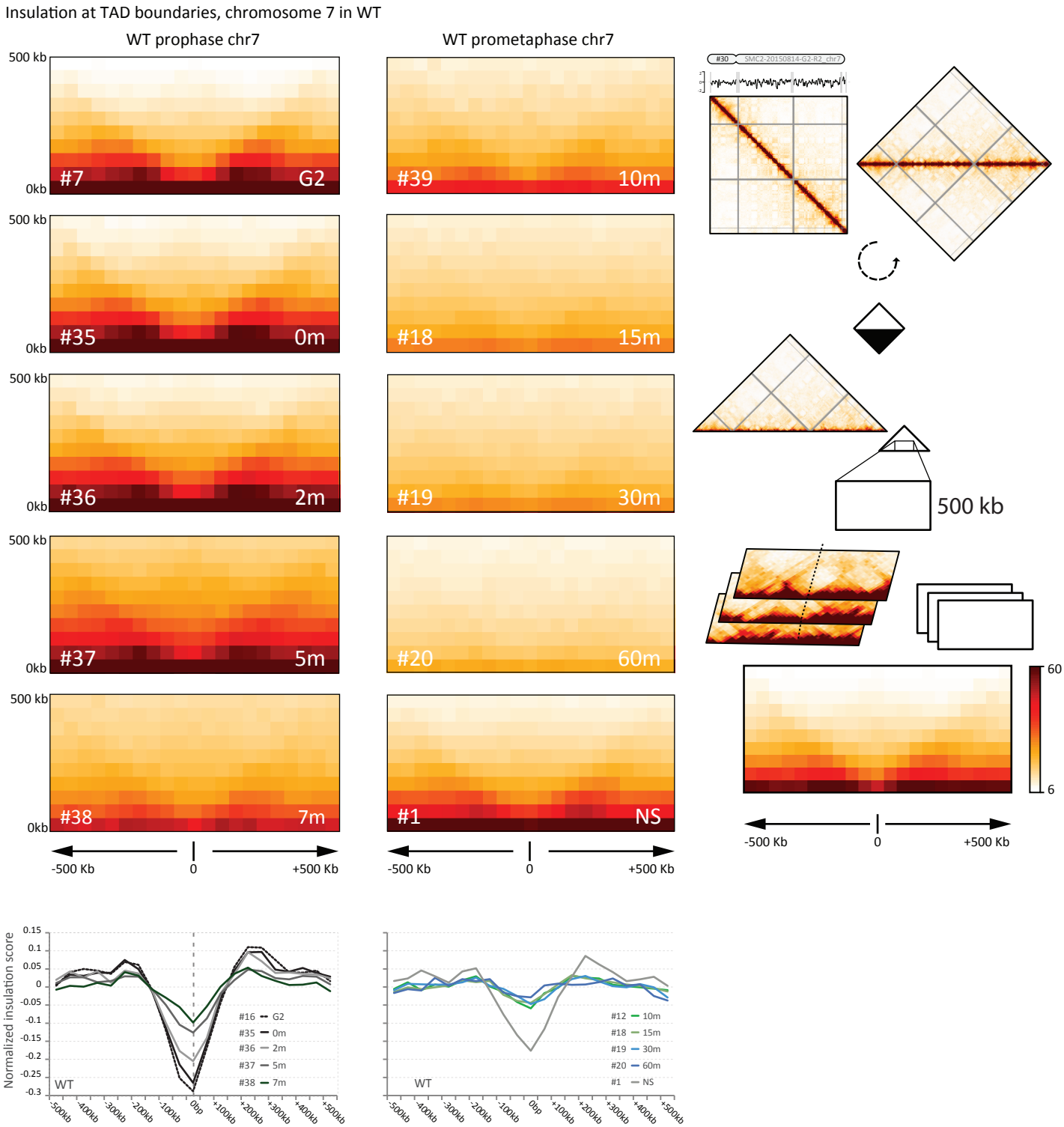
Insulation at TAD boundaries, chromosome 7 in WT
WT prophase chr7
WT prometaphase chr7
500 kb
0kb
#7
G2
#39
10m
#35
0m
#18
15m
#36
2m
#19
30m
#37
5m
#20
60m
#38
7m
#1
NS
-500 Kb
0
+500 Kb
#30
SMC2-20150814-G2-R2_chr7
500 kb
60
6
Normalized insulation score
WT
#16 G2
#35 0m
#36 2m
#37 5m
#38 7m
#12 10m
#18 15m
#19 30m
#20 60m
#1 NS

Fig.S10

A Scaling plots for all WT chromosome arms combined

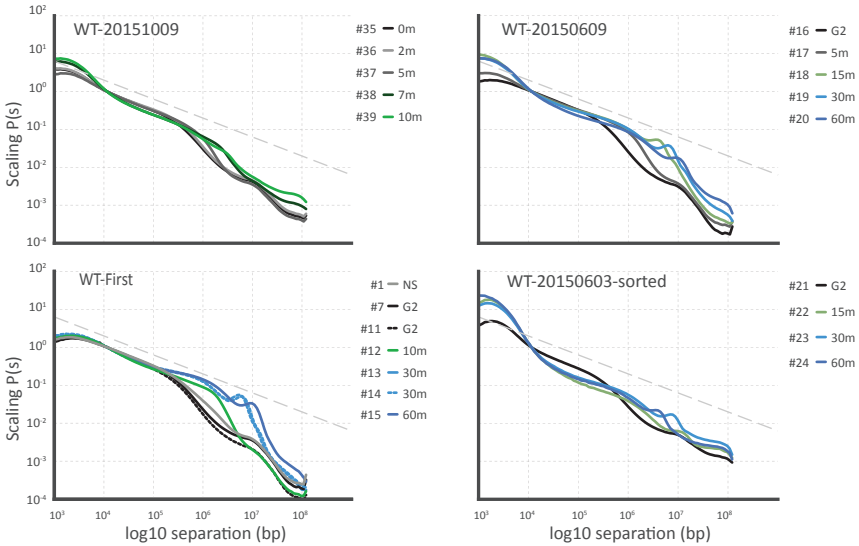

B Scaling derivative plots for all WT chromosome arms combined

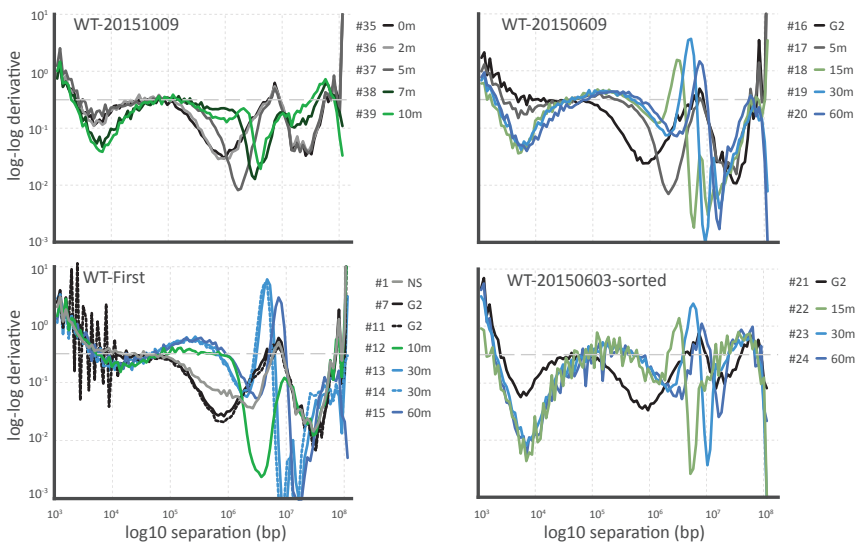

Fig.S11

A Heatmaps, compartments and TADs for HelaS3

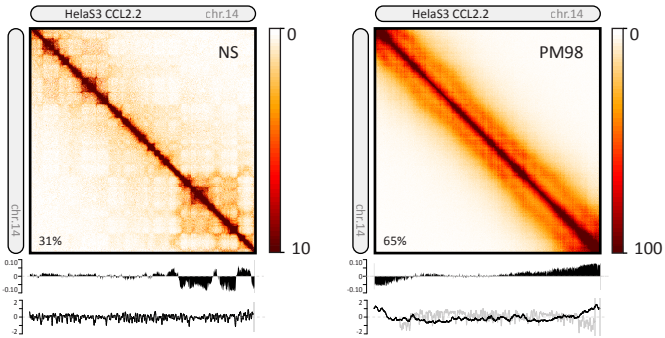

B Scaling plot for HelaS3

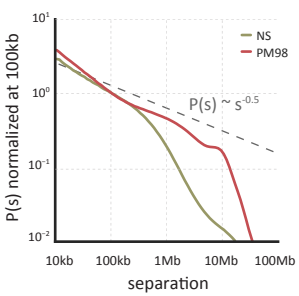

Fig.S12

A Second diagonal not explained by sister overlap

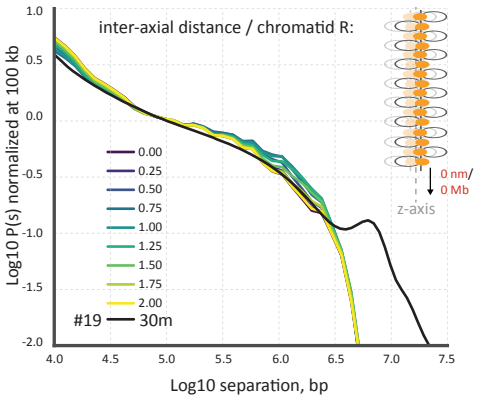

B Without nested loops it does not fit

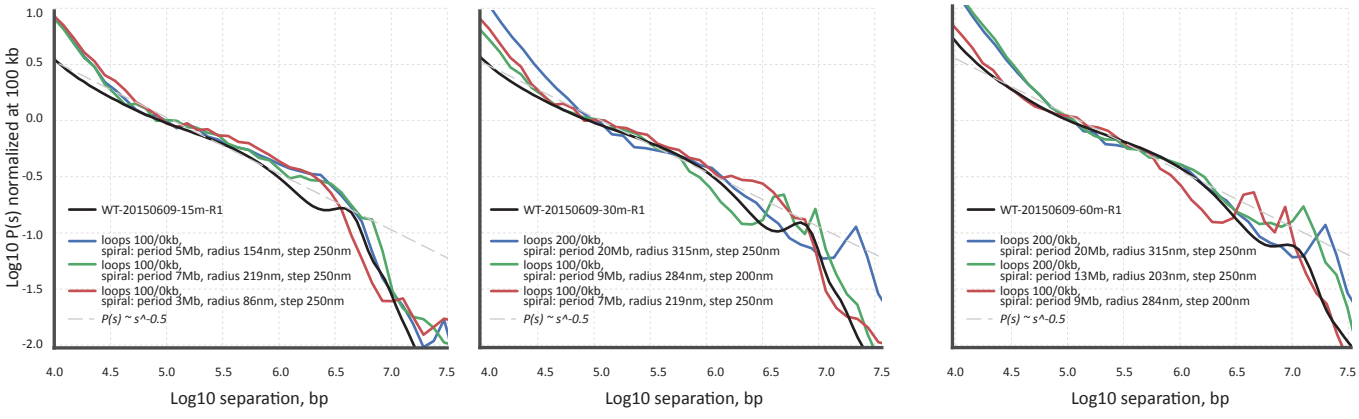

C An external helix does not fit

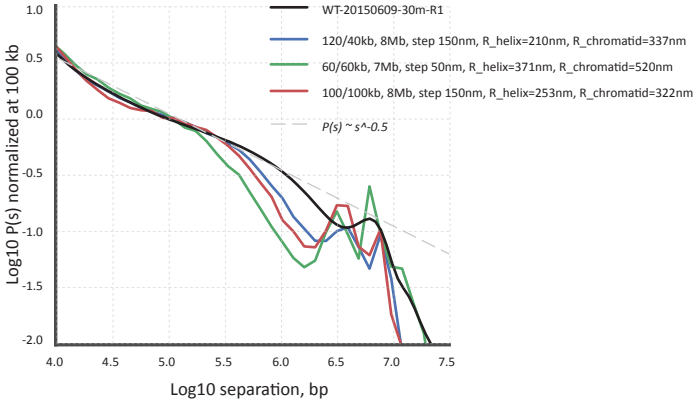

Fig.S13

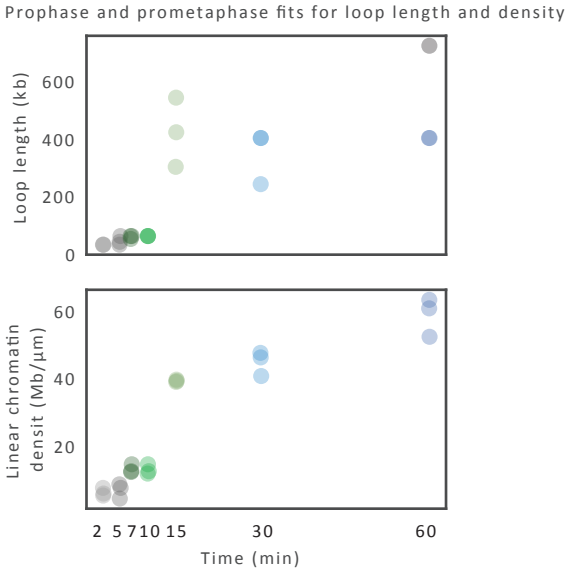
Prophase and prometaphase fits for loop length and density
Loop length (kb)
0
200
400
600
Linear chromatin densit (Mb/µm)
20
40
60
2 5 7 10 15 30 60
Time (min)

Fig.S14

Western blots for auxin induced condensin mutants

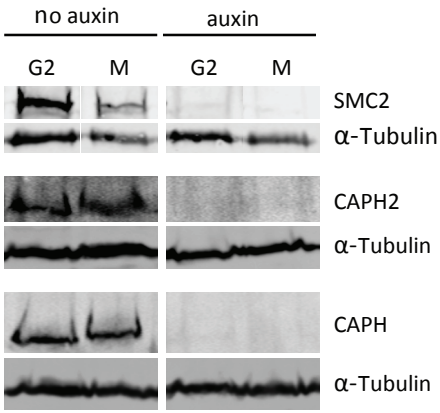

Fig.S15

A Heatmaps from all individual libraries for SMC2-AID chromosome 7

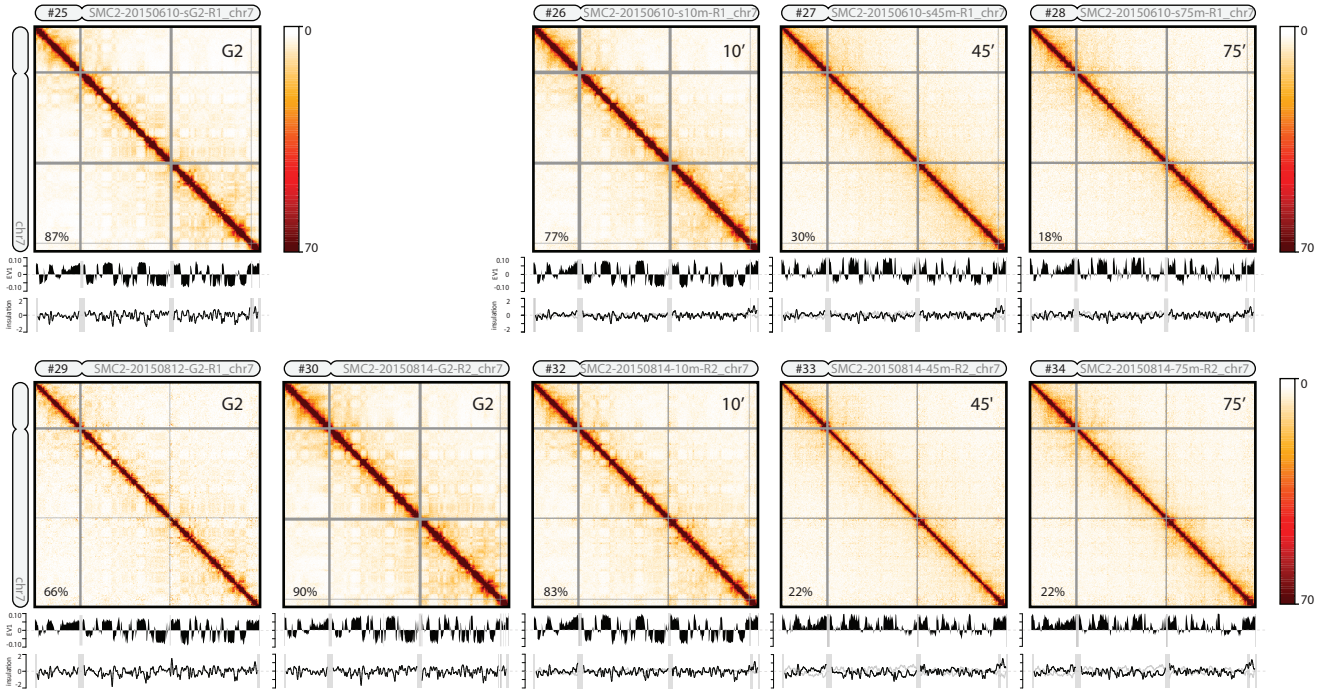

B Heatmaps from all individual libraries for CAPH2AID chromosome 7

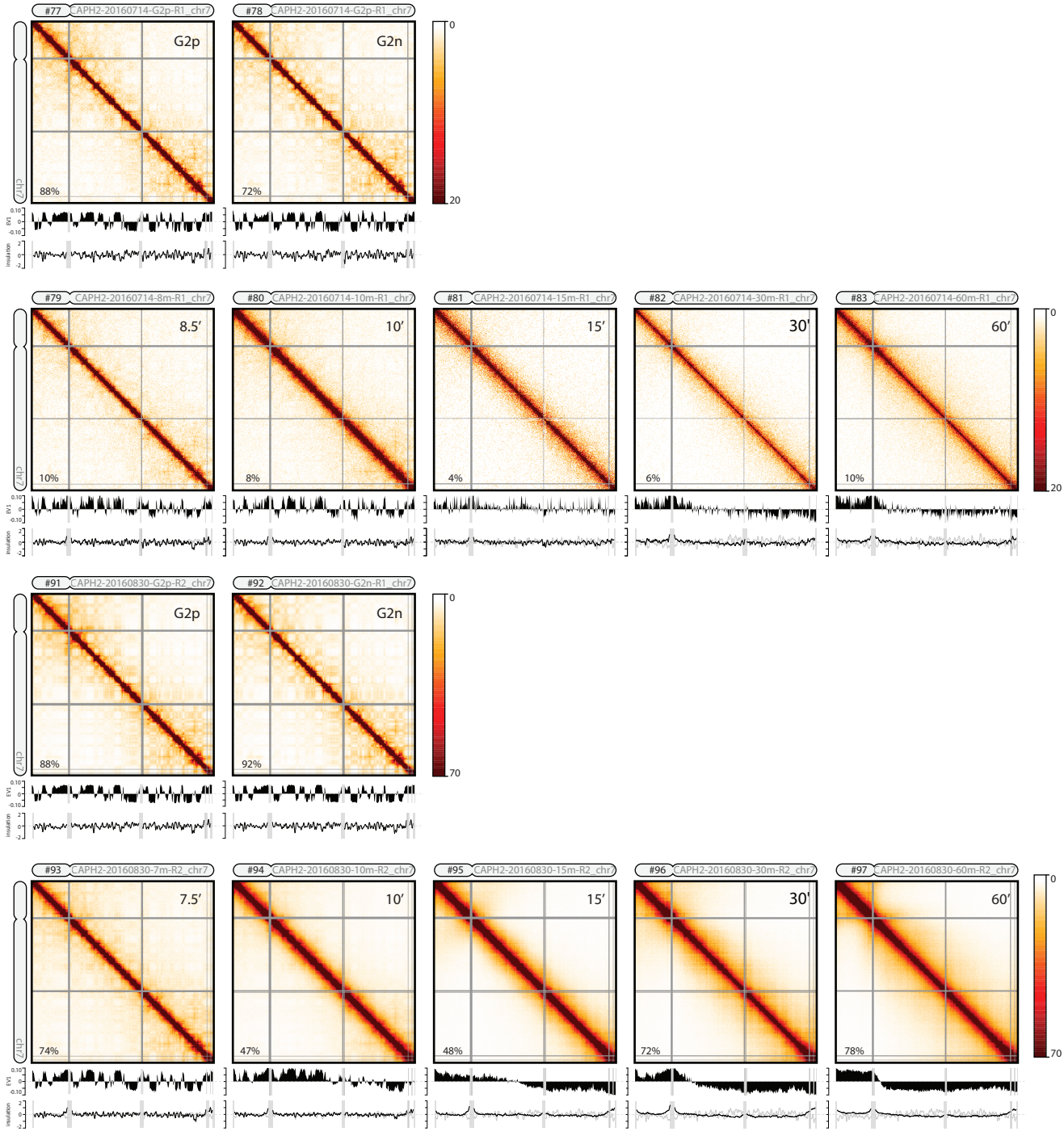

C Heatmaps from all individual libraries for CAPH-AID chromosome 7

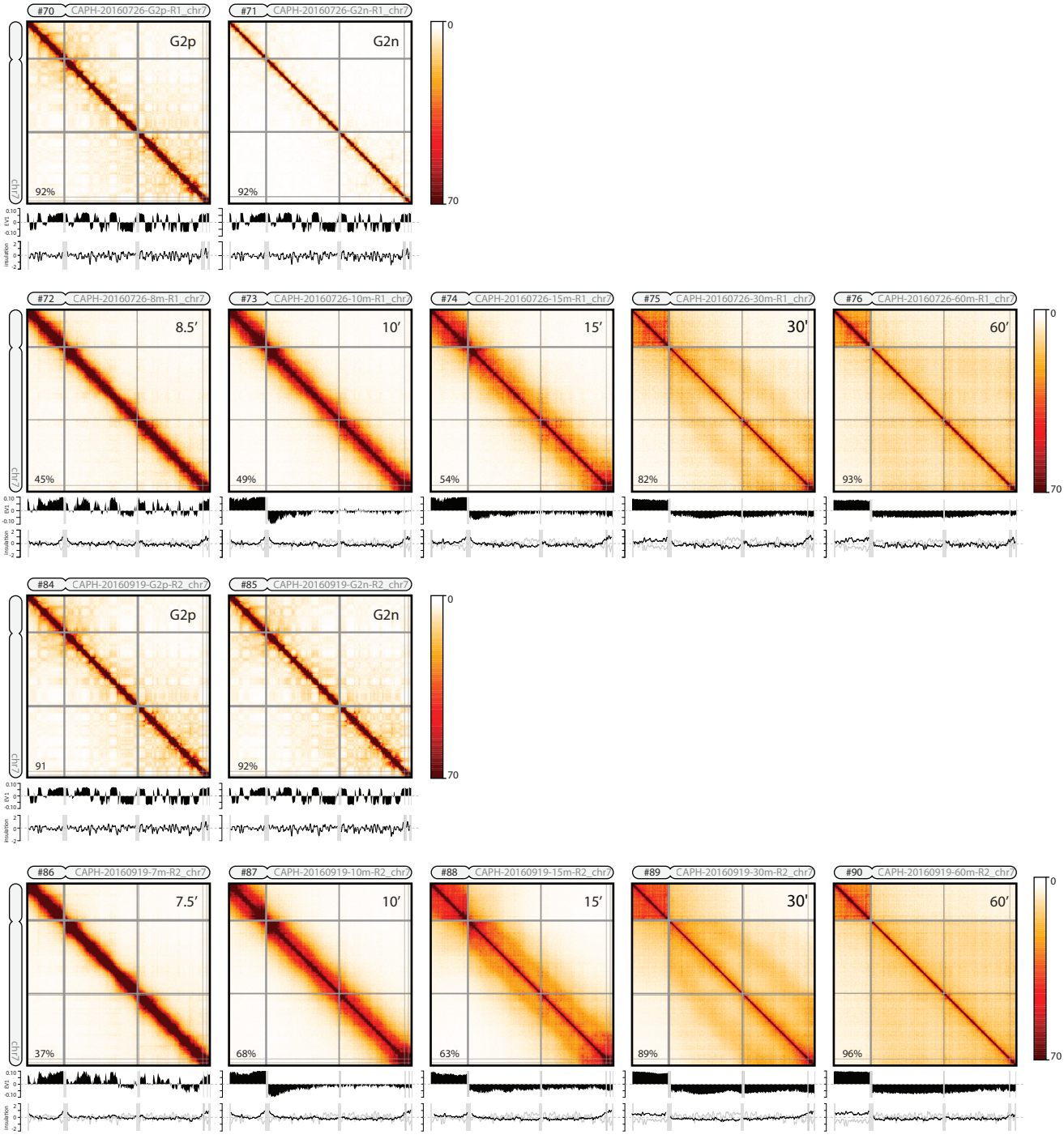

Fig.S16

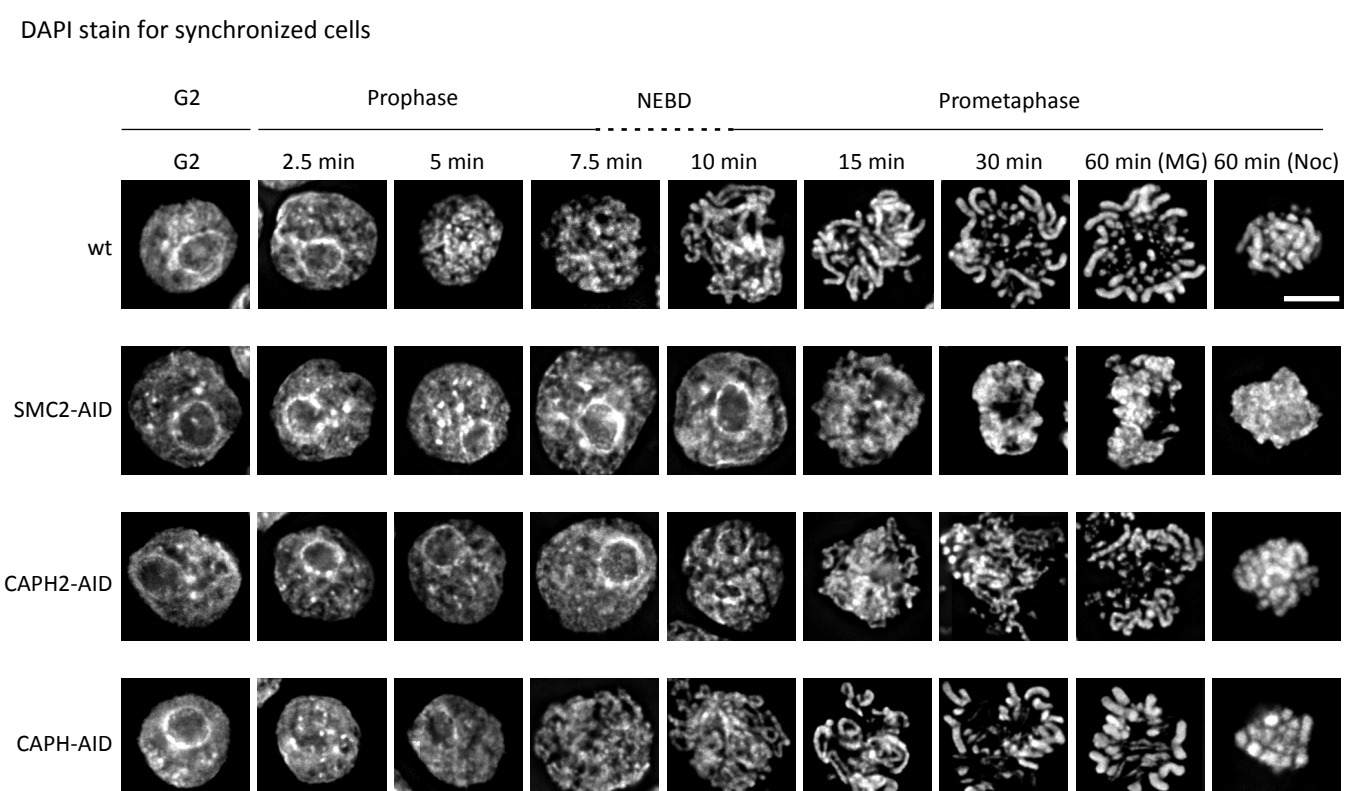
DAPI stain for synchronized cells
G2
Prophase
NEBD
Prometaphase
G2
2.5 min
5 min
7.5 min
10 min
15 min
30 min
60 min (MG)
60 min (Noc)
wt
SMC2-AID
CAPH2-AID
CAPH-AID

Fig.S17

Cumulative variance explained for condensin mutant compartments

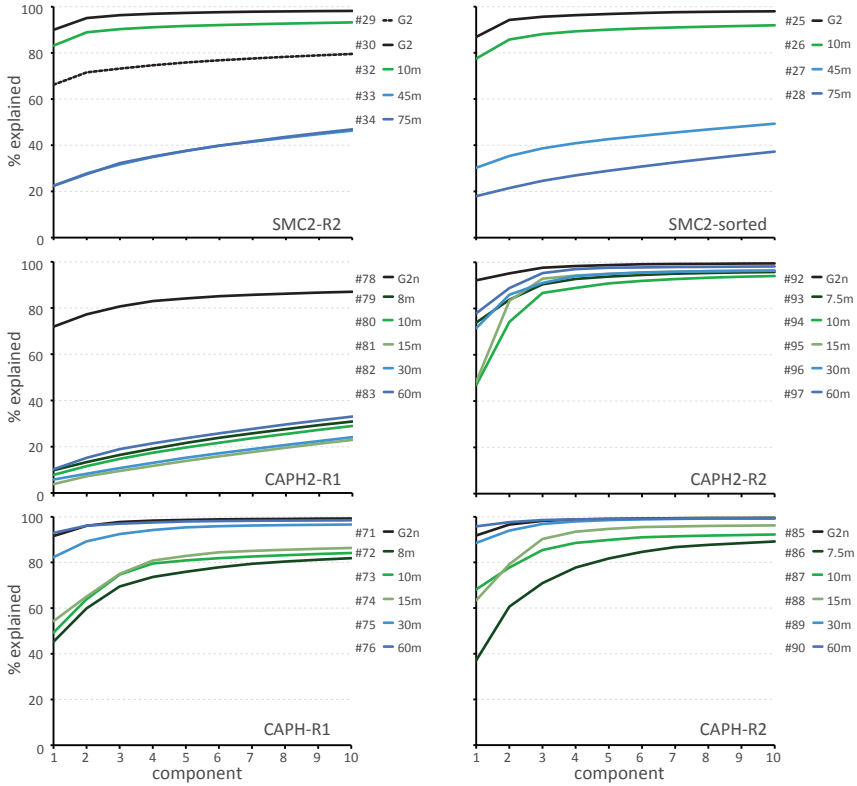

Fig.S18

A

Saddle plots for all individual chromosome arms from SMC2-AID

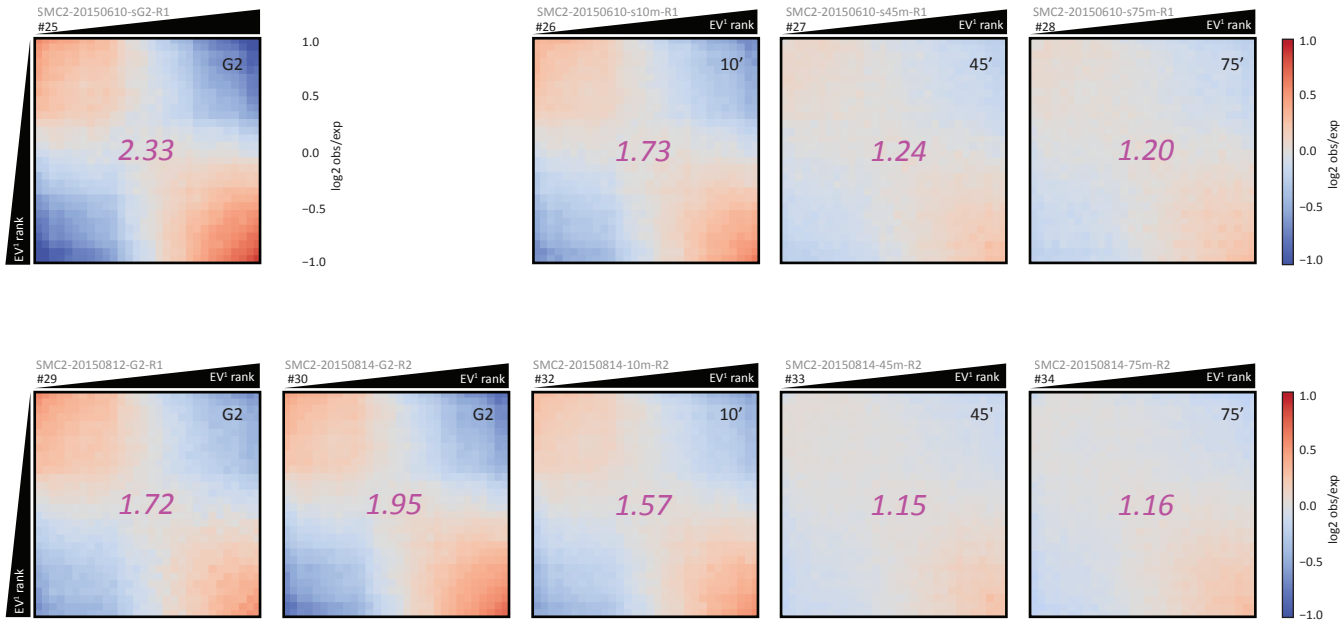

B

Saddle plots for all individual chromosome arms from CAPH2-AID

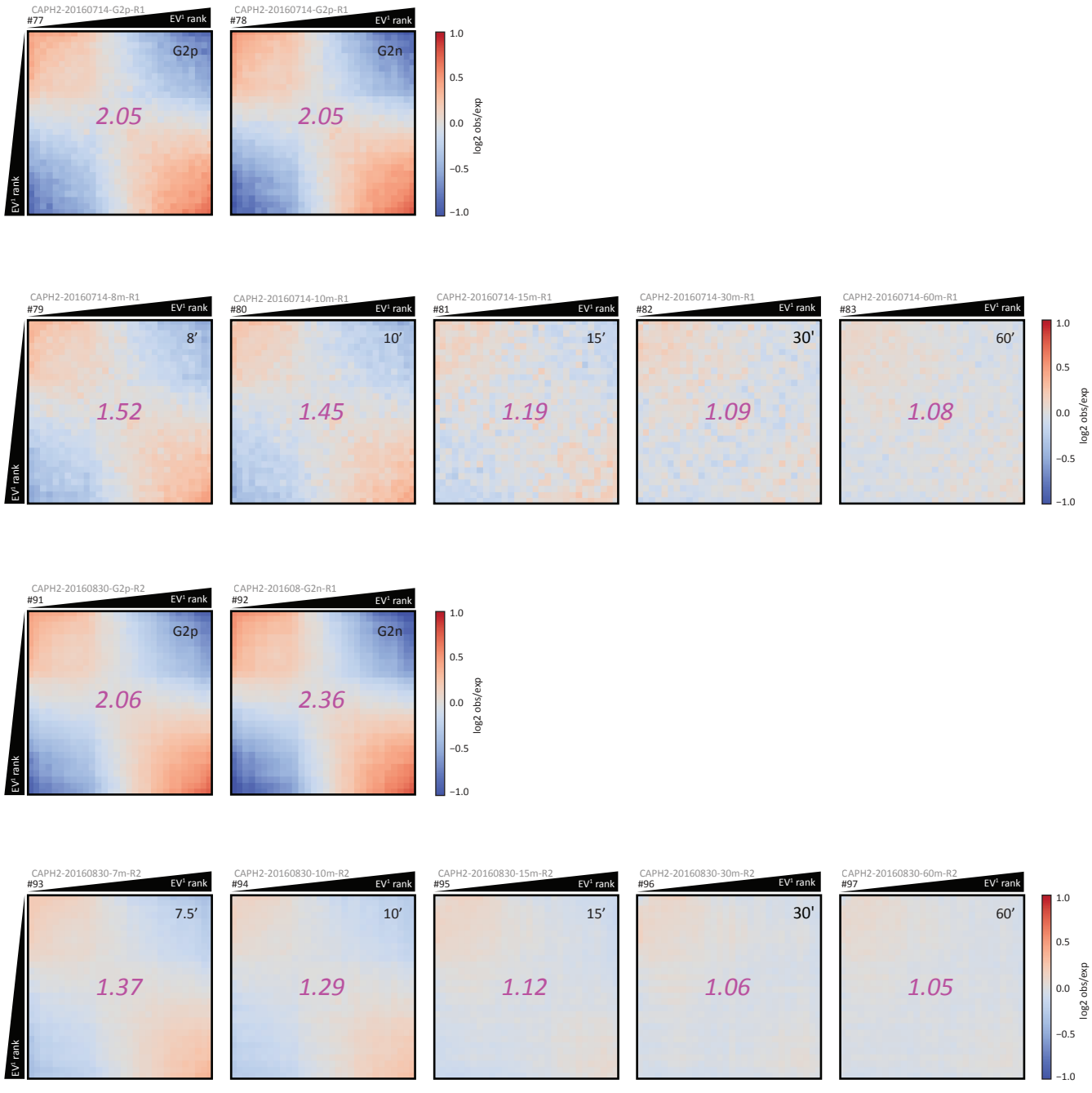

C

Saddle plots for all individual chromosome arms from CAPH-AID

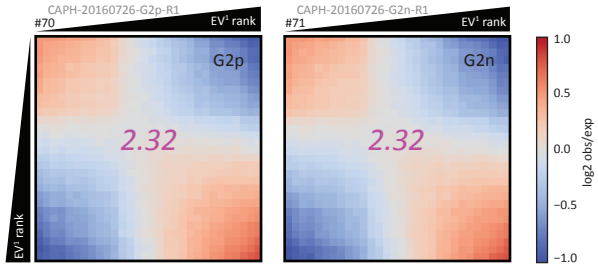

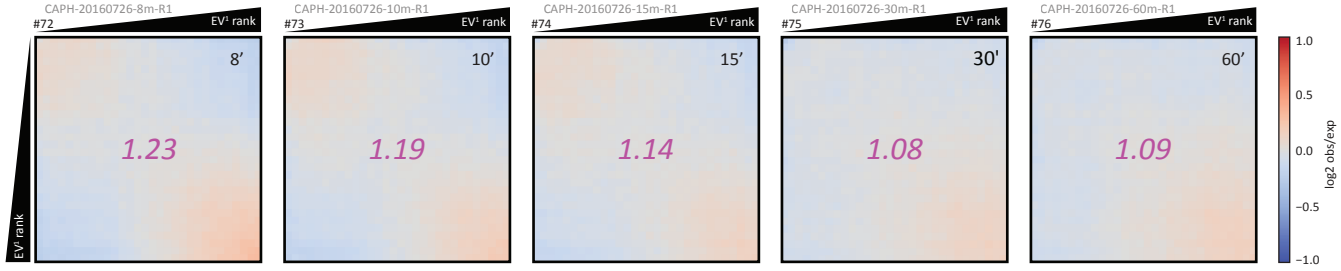

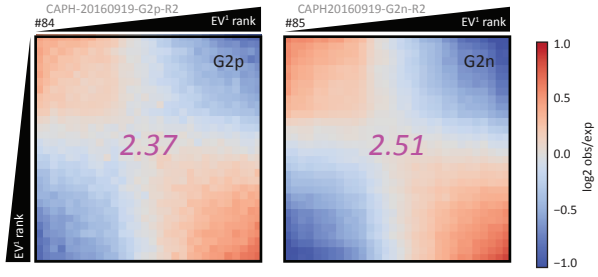

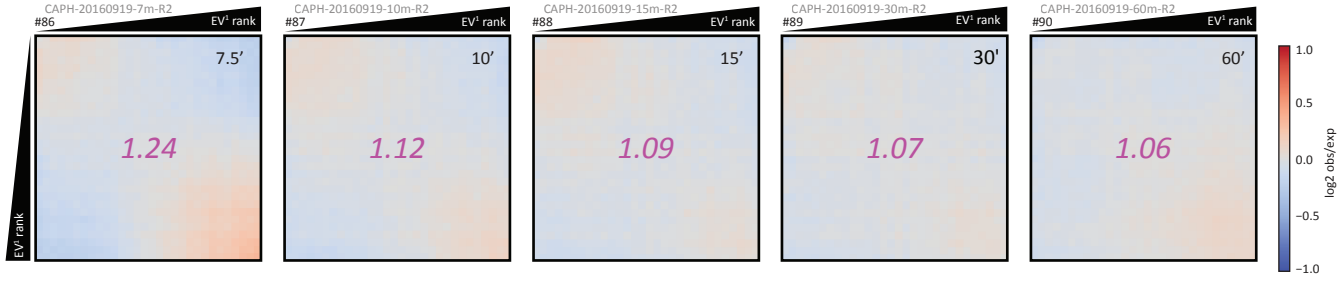

Fig.S19

Insulation at TAD boundaries, chromosome 7 in condensin mutants

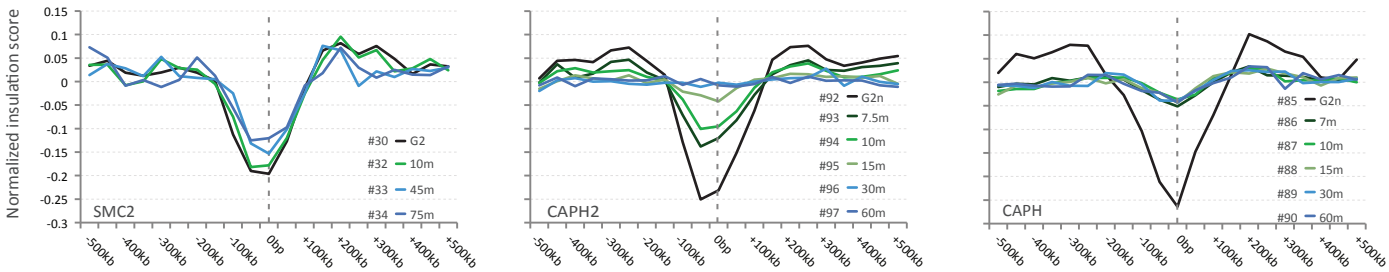

Fig.S20

A SMC2 scaling plots for all individual chromosome arms

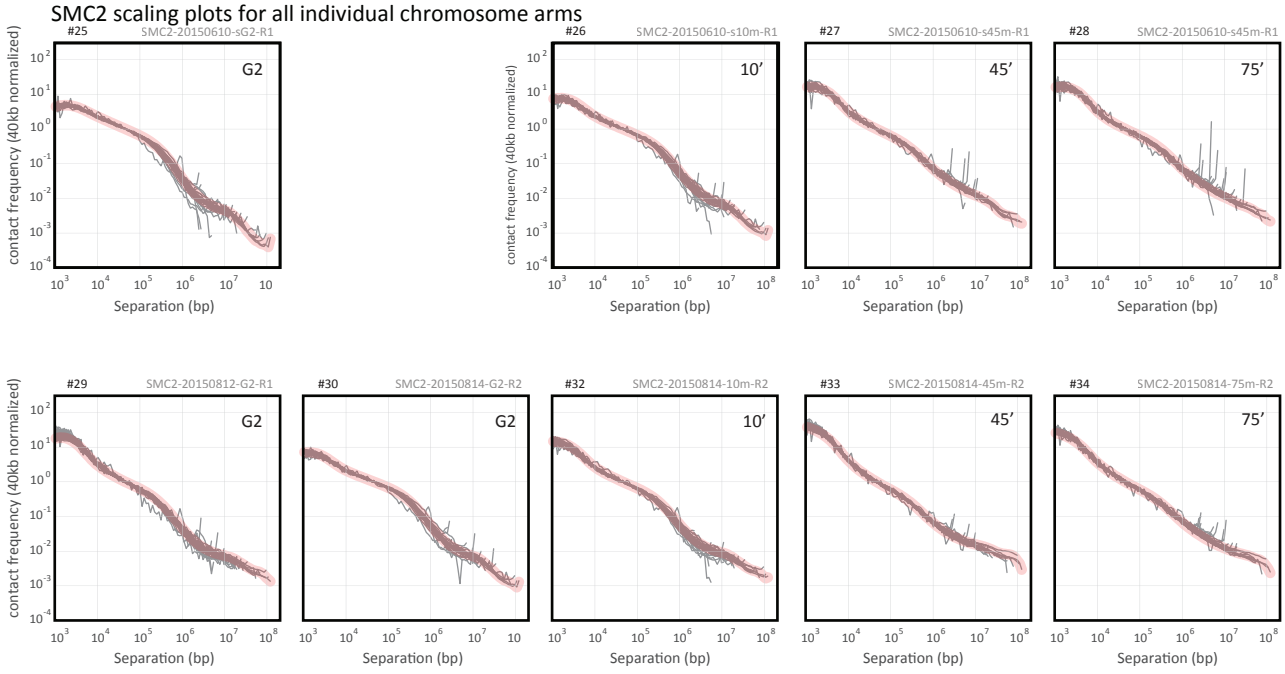

B

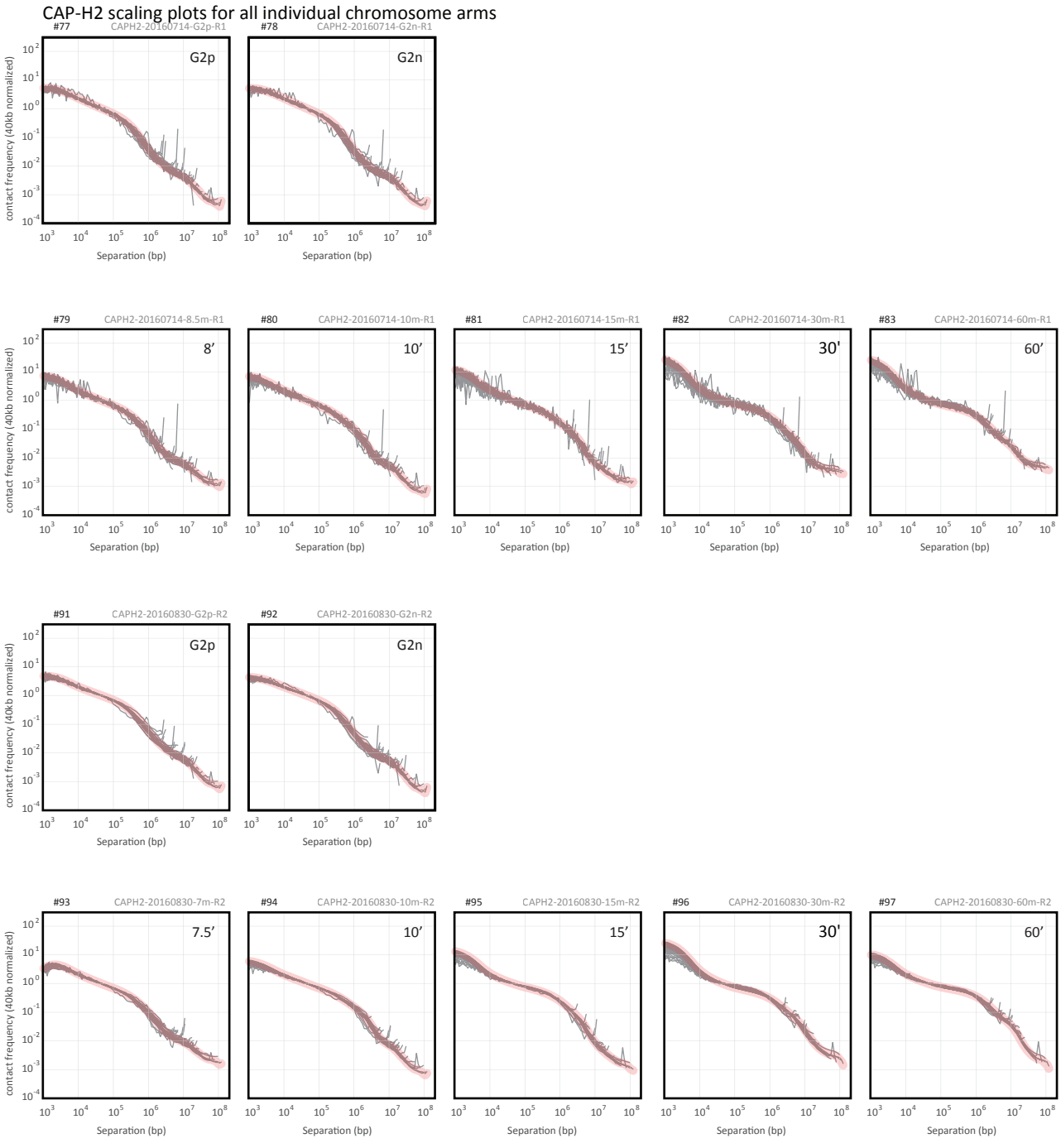
CAP-H2 scaling plots for all individual chromosome arms
#77 CAPH2-20160714-G2p-R1
G2p
#78 CAPH2-20160714-G2n-R1
G2n
#79 CAPH2-20160714-8.5m-R1
8′
#80 CAPH2-20160714-10m-R1
10′
#81 CAPH2-20160714-15m-R1
15′
#82 CAPH2-20160714-30m-R1
30'
#83 CAPH2-20160714-60m-R1
60′
#91 CAPH2-20160830-G2p-R2
G2p
#92 CAPH2-20160830-G2n-R2
G2n
#93 CAPH2-20160830-7m-R2
7.5′
#94 CAPH2-20160830-10m-R2
10′
#95 CAPH2-20160830-15m-R2
15′
#96 CAPH2-20160830-30m-R2
30'
#97 CAPH2-20160830-60m-R2
60′
contact frequency (40kb normalized)
Separation (bp)

C

CAP-H scaling plots for all individual chromosome arms

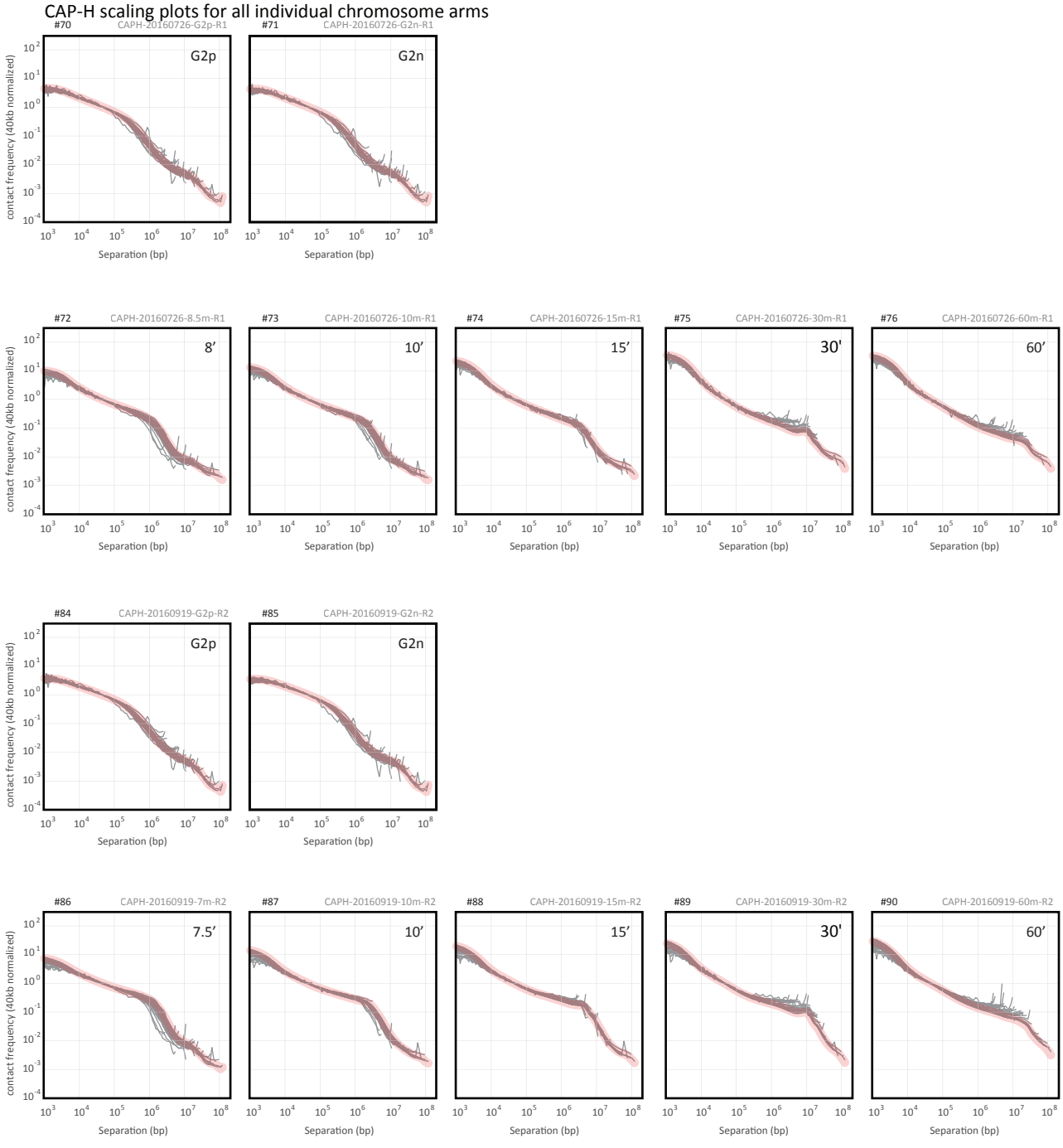

Fig.S21

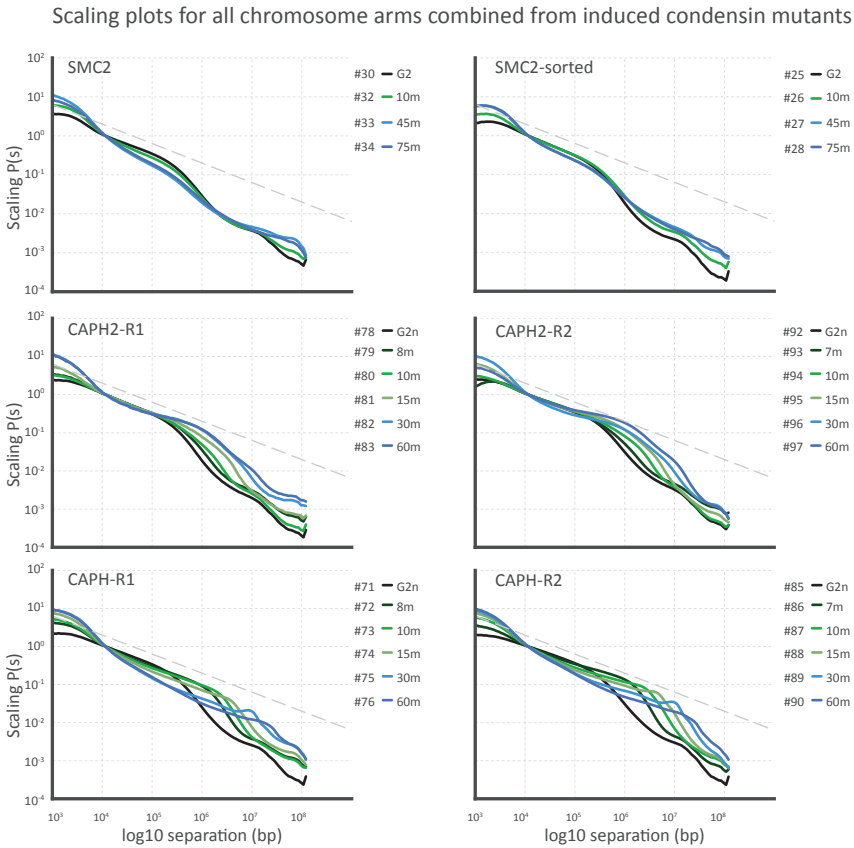
Scaling plots for all chromosome arms combined from induced condensin mutants
SMC2
#30 G2
#32 10m
#33 45m
#34 75m
SMC2-sorted
#25 G2
#26 10m
#27 45m
#28 75m
CAPH2-R1
#78 G2n
#79 8m
#80 10m
#81 15m
#82 30m
#83 60m
CAPH2-R2
#92 G2n
#93 7m
#94 10m
#95 15m
#96 30m
#97 60m
CAPH-R1
#71 G2n
#72 8m
#73 10m
#74 15m
#75 30m
#76 60m
CAPH-R2
#85 G2n
#86 7m
#87 10m
#88 15m
#89 30m
#90 60m
Scaling P(s)
log10 separation (bp)

Fig.S22

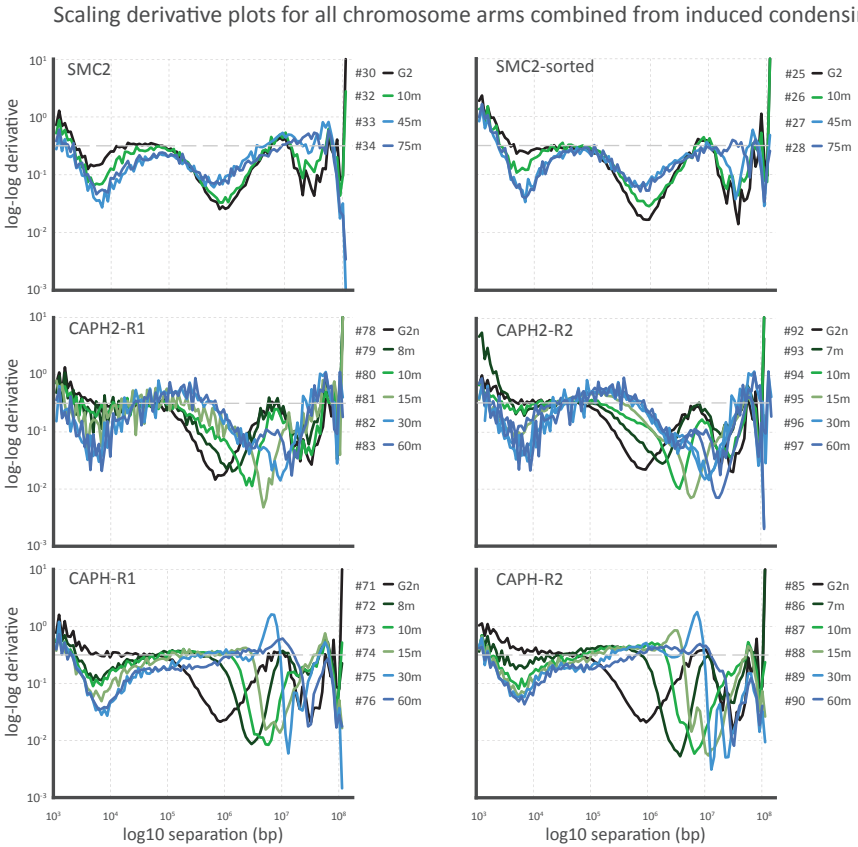
Scaling derivative plots for all chromosome arms combined from induced condensin mutants
SMC2
#30 G2
#32 10m
#33 45m
#34 75m
SMC2-sorted
#25 G2
#26 10m
#27 45m
#28 75m
CAPH2-R1
#78 G2n
#79 8m
#80 10m
#81 15m
#82 30m
#83 60m
CAPH2-R2
#92 G2n
#93 7m
#94 10m
#95 15m
#96 30m
#97 60m
CAPH-R1
#71 G2n
#72 8m
#73 10m
#74 15m
#75 30m
#76 60m
CAPH-R2
#85 G2n
#86 7m
#87 10m
#88 15m
#89 30m
#90 60m
log-log derivative
log10 separation (bp)

Supplementary Materials

Figures S1-S22

Figure S1. FACS analysis for synchronized cell lines. FACS is shown for auxin induced and CDK1as synchronized (10 hr 1NM-PP1) cell lines. Gating was applied for live cells (top-left) and singlets (top-middle) and gated cells were plotted as a histogram for DNA content (top-right). The bottom plot shows the DNA content (DAPI) on the x-axis and time after 1NM-PP1 release (in hours) on the y-axis (top to bottom) for each auxin induced cell line. Cells were not blocked at prometaphase with nocodazole except for the red line (1.0N). This analysis allows determination of the timing for exit from mitosis as a loss of cells in G_2/M (4N peak) and a subsequent increase in cells in the G_1 peak (2N).

Figure S2. Nuclear envelope breakdown (NEBD) in CDK1as synchronized DT40 cells determined by Lamin B1staining. Lamin disassembly and chromosome condensation gradually occur at nuclear breakdown, allowing determining presence of a nuclear envelope. Lamin B1 stains in the nucleus before and throughout the cytoplasm after NEBD (continuous and dotted yellow line respectively). Serine 10 of histone 3 becomes phosphorylated during mitosis (H3K10ph).

Figure S3. Chromatin enriched proteomics (ChEP) data for CDK1as synchronized DT40 cells. Chromatin enrichment for proteomics (ChEP) (*55*) identifies proteins associated with the DNA (see Supplementary Methods). **(A)** Microscopy (DAPI staining of chromosomes) of cells at different time points in mitosis. **(B)** The relative quantitation of chromatin bound condensin I, II and cohesin subunits in CDK1as synchronized cells through WT prophase and prometaphase. Numbers on the y-axis are arbitrary MaxQuant units (in millions), normalized for Histone H4

levels. Timing was made comparable to samples used for microscopy and Hi-C libraries based on cell morphology in (**A**). **(C)** ChEP from CAP-H-AID cells indicates a loss of chromatin bound condensin I subunits after auxin mediated depletion (top). The bottom plot shows the ratio of chromatin binding for CAP-H over CAP-H2 subunits after CAP-H depletion (dotted line) in comparison to 3 replicate control synchronized time course experiments wherein CAP-H was not depleted. **(D)** ChEP for cohesin and CTCF binding on chromatin from auxin induced SMC2-AID and (un-induced) WT. Compared to WT, we find both a reduction in the loss of cohesin and CTCF binding (vertical arrow) and a delay in this reduction (horizontal arrow) for auxin induced SMC2-AID.

Figure S4. Insulation parameter settings for TAD analysis. **(A)** Insulation at different length scales. Hi-C matrices were subjected to insulation analysis (depicted in interaction heatmap below). A square is slid along each diagonal bin of the interaction matrix to aggregate the number of interactions that occur across each bin. Bins with high insulation (at a TAD boundary) have a low insulation score, as measured by fewer interactions within the sliding insulation square. Bins with low insulation or boundary activity (for example, in the middle of a TAD) have a high insulation score. Minima along the insulation profile are potential TAD boundaries. We determined the optimal square size from a range of 50kb to 1Mb to be 250 kb. The large black dotted square (chromatin domain) contains 2 smaller domains structures, indicated by green squares. The specific insulation analyses using 100, 250 and 500 kb windows below the interaction heatmap reveal that small insulation square sizes (<100kb) pick up small scale fluctuations in insulation, whereas larger squares (>500 kb) miss weaker boundaries (green dotted line derived from square above). The line graph in the bottom shows the fluctuation in insulation score for each tested square size (100, 250, 500kb) for the same chromosomal region as the interaction maps above. **(B)** Insulation score variance. The loss of variance in insulation score (galGal5_chr.7) indicates loss of TAD structure after mitotic entry (8).

Figure S5. Contact frequency (*P(s)*) derived from Hi-C data obtained from CDK1as synchronized DT40 cells at different time points in mitosis. **(A)** Contact frequency *P(s)* plots for all WT libraries (two independent time courses). Plots for individual chromosome arms are shown in gray; the deviation from the mean decay is shown in red. The number in the top left refers to library #ID in **Table S2**.

Figure S6. Hi-C data obtained from CDK1as synchronized DT40 cells at different time points in mitosis. Hi-C interaction maps were generated for galGal5 chr.7 normalized to 1,000,000 interactions with a minimum of 0 and a maximum of 70 interactions per 100 kb bin, as indicated by the color scale on the right. Library names are indicated in the chromosome drawing on top left. The number in the top left refers to library #ID in **Table S2**. The top plot below each Hi-C interaction map displays compartment signal (Eigenvector 1; with percentage signal explained by first eigenvector). The bottom graph shows insulation score (TADs). Data for two independent time courses are shown.

Figure S7. Variance of Hi-C data sets explained by the first 10 principal components for four WT datasets at different time points after release from G_2 arrest. On the Y-axis is shown the cumulative percentage of the variance explained by the first 10 principal components (obtained with Principal Component Analysis) for all Hi-C datasets obtained from CDK1as WT DT40 cells at indicated time points after release from G_2 arrest. Hi-C datasets were generated from 4 separate time courses (names in the bottom right). Numbering in the legends refers to dataset ID numbers in **Table S2.**

Figure S8. Quantification of compartment interactions. Bins (100 kb) are arranged by their compartment states (value of eigenvector 1) along both axes and interaction frequencies between them are indicated by the color in the heatmap to produce saddle plots where A-to-A interactiona re represented in the lower right corner and B-to-B interactions are represented in the upper left

corner. Saddle plots were drawn for all Hi-C dataset generated, using the 5-95 percentile of ranked eigen vectors, excluding chromosome 1 and Z. The compartment strength was defined as the median signal from the top 20% of A-A and B-B interactions, divided by the top 20% of A-B interactions ((AA+BB)/2AB). Library names are located on the top left with numbering underneath referring to library ID in **Table S2.**

Figure S9 Insulation values aggregated at G_2 TAD boundaries on chromosome 7 for WT cells at different time points after release from G_2 arrest. Interaction frequency heatmaps show an aggregate of Hi-C interactions 500kb upstream or downstream of TAD boundaries that were defined from insulation analysis on Hi-C data obtained with G_2 arrested CDKas1 WT cells. The aggregation procedure is explained by the schematic on the right. The plots at the bottom show the sum of the interactions for each 100 kb bin 500kb upstream or downstream of the TAD normalized by the average interactions for each timepoint. The presence of a minimum at t = 0 indicates a TAD boundary. As cells progress through mitosis the minimum disappears indicate loss of insulation.

Figure S10 *P(s)* plots and their corresponding derivative plots. *P(s)* plots and their corresponding derivative plots are shown for Hi-C datasets obtained from WT CDK1as cells at indicated time points after release from G_2 arrest.

Figure S11. Hi-C data from HeLaS3 cells arrested in late prometaphase displays a second diagonal. **(A)** Hi-C interaction maps for HelaS3 (ATCC CCL-2.2). (**A**) Hi-C was performed on non-synchronized HelaS3 cells (NS) and HelaS3 cells arrested in late prometaphase with nocodazole, resulting in 98% prometaphase (PM98). Nocodazole synchronization was performed for 3 hrs following a double thymidine block, as described before (8). This Hi-C library was described in (8). The compartment and insulation signals below the interaction frequency heatmaps are as in **Fig. 1**. The values next to the color scale indicate the minimum and maximum number of reads per bin at color saturation. **(B)** *P*(*s)* for HelaS3 NS and PM98 for chromosome

14, as in **Fig. 2**. The dotted line indicates $P(s) \sim s^{-0.5}$ reported before for mitotic chromosomes (8). The local peak in *P(s)* around 10 Mb corresponds to the second diagonal band visible in the Hi-C interaction map (**A**).

Figure S12. Polymer models that do not produce *P(s)* plots consistent with experimental Hi-C data. **(A)** Sisters chromatid overlap does not explain second diagonal formation. **(B)** Nested loops are necessary to fit prometaphase *P(s)*. **(C)** Simulation of an external helix does not produce P(s) that corresponds to experimental prometaphase Hi-C data. Black lines: experimental Hi-C data (dataset indicated in the legend). Colored lines; P(s) plot obtained by simulations with different parameter (indicated in the legend).

Figure S13. Parameters of best fitting models as a function time after release from G2 arrest. Chromatin density and loop length increase linearly from prophase through prometaphase.

Figure S14. Western blots showing protein levels of SMC2, CAP-H and CAP-H2 for respective AID-containing cell lines with or without auxin incubation. Western blots indicate SMC2-AID, CAP-H-AID and CAP-H2-AID are efficiently depleted after 3 hours of incubation in the presence of auxin without and after auxin addition.

Figure S15. Hi-C interaction maps obtained from SMC2, CAP-H and CAP-H2 depleted cells at different time points after release from G_2 arrest. Hi-C interaction maps were generated for galGal5 chr.7, normalized to 1,000,000 interactions with a minimum of 0 and a maximum of 70 interactions per 100 kb bin, as indicated by the color scale on the right. Dataset names are indicated in the chromosome drawing on top. The number in the top left refers to library #ID in **Table S2**. (**A**): SMC2-AID cells; (**B**): CAP-H2-AID cells; (**C**): CAP-H-AID cells. The top plot below each Hi-C interaction map displays compartment signal (Eigenvector 1; with percentage

signal explained by first eigenvector). The bottom graph shows insulation score (TADs). Data for two independent time courses are shown.

Figure S16. Microscopy analysis of chromosome morphology for wild type (WT) cells and SMC-AID, CAP-H2-AID and CAP-H-AID cells after auxin-induced depletion of AID-containing proteins at indicated time points after release from G_2 arrest. Chromosomes were stained with DAPI. Samples are ordered by time of harvest after release from G2 arrest NEBD was used a marker for the prophase-prometaphase transition. Cells were prevented from entering anaphase by addition of nocodazole or MG132. Scale bar indicates 5 micron. CAPH: CAP-H-AID; CAPH2: CAP-H2-AID; SMC2: SMC2-AID; Noc: nocodazole; MG: MG132.

Figure S17. Variance of Hi-C data sets explained by the first 10 principal components for SMC2, CAP-H and CAP-H2 depleted cells at different time points after release from G_2 arrest. On the Y-axis is shown the cumulative percentage of the variance explained by the first 10 principal components (obtained with Principal Component Analysis) for all Hi-C datasets obtained from auxin treated cultures of SMC-AID, CAP-H-AID and CAP-H2-AID cells at indicated time points after release from G_2 arrest. Names of the Hi-C datasets are indicated in the bottom right of each plot. Data for two independent replicate timecourses (R1 and R2) are shown. Numbering in the legends refers to dataset ID numbers in **Table S2.**

Figure S18. Quantification of compartment interactions in SMC2, CAP-H and CAP-H2-depleted cells at different time points after release from G_2 arrest. (**A**): SMC2-AID cells; (**B**): CAP-H2-AID cells; (**C**): CAP-H-AID cells. Bins (100 kb) are arranged by their compartment states (value of eigenvector 1) along both axes and interaction frequencies between them are indicated by the color in the heatmap to produce saddle plots where A-to-A interactiona re represented in the lower right corner and B-to-B interactions are represented in the upper left corner. Saddle plots were drawn for all indicated Hi-C dataset generated, using the 5-95 percentile of ranked eigen vectors, excluding chromosome 1 and Z. The compartment strength was defined as the median

signal from the top 20% of A-A and B-B interactions, divided by the top 20% of A-B interactions ((AA+BB)/2AB). Library names are located on the top left with numbering underneath referring to library ID in **Table S2.**

Figure S19. Insulation values aggregated at G_2 TAD boundaries on chromosome 7 for cells depleted for SMC2, CAP-H2 or CAP-H at different time points after release from G_2 arrest. Interaction frequency heatmaps show an aggregate of Hi-C interactions 500kb upstream or downstream of TAD boundaries that were defined from insulation analysis on Hi-C data obtained with G_2 arrested CDKas1 cells expressing SMC2-AID, CAP-H2-AID or CAP-H-AID. plots show the sum of the interactions for each 100 kb bin 500kb upstream or downstream of the TAD normalized by the average interactions for each time point. The presence of a minimum at t = 0 indicates a TAD boundary. SMC2 depletion prevents complete loss of the minimum, indicated maintenance of TAD boundaries. Depletion of CAP-H2 leads to slower loss of TAD boundaries as compared to WT (**Fig. S9**). Depletion of CAP-H does not prevent efficient loss of TAD boundaries.

Figure S20. Contact frequency (*P(s)*) derived from Hi-C data obtained from CDK1as synchronized DT40 SMC2-AID, CAP-H2-AID or CAP-H depleted cells at different time points in mitosis. (**A**): SMC2-AID cells; (**B**): CAP-H2-AID cells; (**C**): CAP-H-AID cells. Contact frequency *P(s)* plots for all Hi-C datasets (two independent time courses). Plots for individual chromosome arms are shown in gray; the deviation from the mean decay is shown in red. The number in the top left refers to library #ID in **Table S2**.

Figure S21. *P(s)* plots for SMC2-AID, CAP-H2-AID and CAP-H-AID DT40 cells at different time after degron induction and release from G2 arrest. *P(s)* plots for Hi-C datasets corresponding to each time course experiment are plotted in one graph. The number in the top right refer to dataset #ID in **Table S2**.

Figure S22. Derivatives of *P(s)* plots for SMC2, CAP-H2 or CAP-H depleted cells at different time point after release from G_2 arrest. Plots show derivative of *P(s)* plots for Hi-C datasets obtained from SMC2-AID, CAP-H2-AID and CAP-H CDK1as cells at indicated time points after auxin-induced protein depletion and release from G_2 arrest.

Tables S1-S3.

Table S1. Sample and FACS summary. All samples with their cell type used for Hi-C libraries (name_galGal5) are listed with a unique number (#ID) that refers to the same #ID used throughout all figures. For each cell collection (time), the main cell cycle phase, treatments and drugs used are listed. FACS analysis was used to determine AID-GFP presence (and level of protein degradation). A subset of cells was sorted (sorted) for GFP positivity or negativity respectively, as indicated.

Table S2. Hi-C dataset overview. The unique number (#ID) corresponds with the #ID from figures and **Table S1**. Each harvested cell sample was submitted to Hi-C as part of a set (Set#) and the sequencing results and mapping statistics for galGal5 (gg5) are listed. Valid pair: reads mapped for both ends; NRVP (non-redundant valid pairs): valid pairs with duplicate reads removed (see Supplementary Methods); %Dangling: percentage of dangling ends (inward reads [→|←] derived from false biotin incorporation); %cis: percentage of intra-chromosomal interactions; %redundant: percentage of exact (PCR) duplicate reads (used to determine NRVP).

Table S3. DNA constructs used for generation of cell lines. Mutant: name used throughout the manuscript; background: cell line used to generate modified cell line; construct: vector used to generate mutants; FBOX: the specific FBOX protein used to degrade the AID-fused mutant; endogenous: the modification to the endogenous locus using homologous recombination (HR) or

CRISPR; alleles: the number and location of altered alleles in DT40 mutants; selection: antibiotic resistance used for mutant selection; publication: previous work using these mutants.

Supplementary Materials and Methods:

Cell culture

Chicken DT40 (B-cell lymphoma) cells were cultured in RPMI 1640 medium supplemented with 10 % fetal bovine serum and 1% chicken serum at 39°C in 5% CO2 in air.

Stable transfection into DT40 cells was performed as described previously (22). Transient transfection into DT40 cells was performed using a Neon transfection system from ThermoFisher Scientific. 2-4 million cells suspended in 100 µl 1X buffer R were mixed with plasmid DNA (4-10 µg), then electroporated at setting 5.

Doxycycline (BD) dissolved in water (1mg/ml) was added to a final concentration of 0.5 µg/ml. For G_2 arrest, 1NM-PP1 dissolved in DMSO (10 mM) was added to cultures at a final concentration of 2 µM. Degradation of AID-containing proteins was induced by addition of a 50 mM solution of Indole-3-acetic acid (auxin, Fluka) dissolved in ethanol to a final concentration of 125 µM. To prevent cells from entering anaphase, Nocodazole (Sigma-Aldrich) dissolved in DMSO at 1 mg/ml was added to some cultures to a final concentration of 0.5 µg/ml (see details below, **Table S1**).

Cell lines

A summary of the cell lines described below can be found in **Table S3**.

SMC2-AID-GFP cells: SMC2-AID-GFP cells were derived from a previously described SMC2 conditional (doxycycline induced) knockout cell line (51). Plasmids coding SMC2-mAID-GFP and OsTIR1 were randomly integrated into the DT40 genome. A 3.8 kb fragment of the endogenous GgSMC2 promoter (51) drove expression of the GgSMC2 cDNA fused with a minimal AID (mAID) tag (AtIAA1765-132) and GFP tag (SMC2-mAID-GFP) at the C-terminus. A CMV promoter drove the expression of plant-specific F-box protein OsTIR1 linked to a MmDHFR cDNA by a T2A peptide (synthesized at Thermofisher Scientific and cloned into pCDNA3). 10 µM Methotrexate (MTX) was used to select cells expressing high levels of

MmDHFR and OsTIR1. The resultant cell lines (named SMC2-AID-GFP) were cultured continuously in the presence of doxycycline (0.5 μg/ml) to suppress the expression of non-tagged GgSMC2 protein.

CAP-H-AID-GFP cells: Plasmids encoding CAP-H-mAID-GFP and plant specific F-box protein OsTIR1 were randomly integrated into the genome of a CAP-H conditional (doxycycline induced) knockout cell line (*58*). A CMV promoter drove the expression of the GgCAP-H-mAID-GFP. A CMV promoter drove the expression of OsTIR1 linked to a MmDHFR cDNA by a T2A peptide (synthesized at Thermofisher Scientific and cloned into pCDNA3). 10 μM Methotrexate (MTX) was used to select cells expressing high levels of MmDHFR and OsTIR1. The resultant CAP-H-AID-GFP cell lines were cultured continuously in the presence of doxycycline (0.5 μg/ml) to suppress the expression of non-tagged GgCAP-H protein.

CAP-H2-AID-GFP cells: CAP-H2-AID-GFP cells were constructed starting with wild type DT40 cells. A codon-optimized GgCAP-H2 cDNA was synthesized (Thermofisher Scientific) and cloned into pAID2.3C so that CAP-H2 was tagged with mAID and GFP at its C-terminus. A CMV promoter drove the co-expression of OsTIR1 and CAP-H2-mAID-GFP, which are linked by a P2A peptide in the pAID2.3C-CAP-H2 plasmid. The pAID2.3C-CAP-H2 plasmid was randomly integrated into the DT40 genome. The endogenous GgCAP-H2 gene was then inactivated by transient transfection of plasmids encoding hCas9 cDNA and GgCapH2 guide RNA (Thermofisher Scientific). The target sequence of guide RNA was CCTATACTCGCTGGTCTACCAGG.

CDK1as cells: A CMV promoter drove the expression of a XlCdk1as cDNA (21) linked to a puromycin or zeocin resistance gene via a T2A peptide. This construct was integrated at random in the genome of the desired target cell line. The endogenous GgCdk1 gene was then inactivated by transient transfection of plasmids encoding hCas9 cDNA (Addgene #41815) and GgCdk1 guideRNA (based on Addgene #41824). The target sequence of the guide RNA was AAAATACGTCTAGAAAGTG. SMC2-AID-GFP cells, CAP-H-AID-GFP cells and CAP-H2-AID-GFP cells were individually converted into CDK1as cell lines by this method. Wild type CDK1as cells were a gift of Helfrid Hochegger (University of Sussex) (21).

Detailed protocols to establish DT40-AID/CDK1as cell lines are available upon request to Dr. Kumiko Samejima.

Time course experiments

Typically 1-3 x10^7 CDK1as wild type cells/sample were treated with 1NM-PP1 (final concentration: 2 μM) for 10 h, after which over 95% were in G2 (**Fig. S15**). G_2-arrested cells were collected prior to 1NM-PP1-washout. To release cells from the G_2 arrest, 1NM-PP1 was washed out by collecting the cells by centrifugation (1300 rpm, 2-5 min - depending on the volume of cultured cells - at RT) and suspending the cells in fresh media (10-20 ml). Cells were washed twice over a period of 10-20 minutes (this varied depending on the number of cultures being processed simultaneously). These cells were suspended in fresh media and divided into flasks (one flask for each time point, typically 1-3 x10^7 cells per flask) and returned to the incubator (counted as t = 0 minutes). At each time point (0, 2.5, 5, 7.5, 10, 30, 45, 60, 75 minutes), a flask was removed from the incubator and cells with media were transferred to a 50 ml Falcon tube, which was topped up with fresh media to 45 ml.

3 ml of 16% formaldehyde solution was added to the 50 ml tube to obtain a final concentration of 1%. The content was quickly mixed by inverting the tube twice and left at RT for 10 min for cross-linking. 2.5 ml of 2.5 M glycine was then added to the tube to stop cross-linking. The content was quickly mixed by inverting the tube twice and left at RT for 5 min, and then on ice for at least 15 min. Subsequently, cells were collected by centrifugation (2000 rpm, 10 min), and the cell pellet was frozen on dry ice and then stored at -80°C.

Modifications to the time course experiment

Auxin-induced protein depletion

Where required, auxin was added after 10 h 1NM-PP1 treatment and cells (SMC2-AID-GFP cells, CAP-H-AID-GFP cells, CAP-H2-AID-GFP cells) were further incubated for 3 h to deplete AID-tagged proteins. Cells were then released from the G2 arrest as described above, except that auxin was kept in the 1NM-PP1 washout media and in the media during all further incubations. Note that the terms "G_2n" (G_2 GFP negative) and "G_2p" (G_2 GFP positive) for samples for CAPH1 and CAPH2 listed in Table S1, S2 refer to addition of auxin and subsequent degron

activity. G_2n had auxin added (degron active), whereas G_2p had no auxin added (degron not activated).

Cell sorting to isolate cells depleted of target proteins

As a control, in some cases (indicated as "sorted") SMC2-AID-GFP cells were cell sorted after cross-linking to exclude residual GFP-positive cells, which had not responded fully to auxin. Some wild type cells were also sorted. Sorting did not alter the Hi-C data as compared to unsorted cells, indicating that degron-mediated protein degradation was very efficient (**Fig. 4A, S2, S16**).

Nocodazole addition to prevent anaphase entry

Nocodazole was added for 30 minutes prior to 1NM-PP1 washout only for the $t \geq 30$ minute time points (Replicate 1 of WT) or for $t \geq 60$ minutes samples (all other time courses; **Table S1**). Nocodazole was present in 1NM-PP1 washout media and in the media during further incubations. No nocodazole was added for cells collected at any of the other time points.

Microscopy on fixed cells

Fixation of chromosomes from mitotic cells

Cells in media (200 µl) were directly fixed in 1 ml of ice-cold Methanol/Acetic acid solution (3:1) for > 30 minutes. Fixed Cells were centrifuged at 2000 g for 1 min, applied on slides, air dried, and stained with DAPI in Vectashield antifade mounting medium (H-1200, Vectashield). Images were taken by DeltaVision microscopy.

Lamin B1 and Histone H3 Phos-Ser10 staining

Cells were fixed in pre-warmed 4 % Formaldehyde/PBS for 10 min and permeabilized with 0.15 % triton for 5 minutes. The following steps were then performed at room temperature. Cells were blocked with 5 % BSA/PBS for 30 minutes. Anti-lamin B1 mouse monoclonal antibody (1:100,

Zymed) and Anti-histone H3 phospho-Ser10 rabbit polyclonal antibody (1:500, Millipore) diluted in the blocking buffer were applied to the cells for 1 hour. Cells were washed with PBS 3x for 5 minutes. Secondary antibodies (Molecular Probes, ThermoFisher Scientific) anti-mouse and anti-rabbit coupled with Alexa Fluor 488 and 594, respectively and diluted 1:500 and 1:1000 in the blocking buffer, were applied to the cells for 30 minutes. Cells were washed with PBS three times for 5 minutes. DNA was stained with Hochest33452 and mounted with Prolong diamond (Molecular Probes, ThermoFisher Scientific). Images were taken by DeltaVision microscopy.

DeltaVision microscopy

3D datasets were acquired using a cooled CCD camera (CoolSNAP HQ; Photometrics) on a wide-field microscope (DeltaVision Spectris; Applied Precision) with a 100× NA 1.4 Plan Apochromat lens. The datasets were deconvolved with softWoRx (Applied Precision), converted to Quick Projections in softWoRx, exported as TIFF files, and imported into Adobe Photoshop for final presentation.

Immunoblot analysis

Typically 0.5-1 x 10^6 cells were loaded in each lane of a 7.5 % SDS-PAGE gel. Proteins were transferred to PVDF membranes at 200 mA for 2.5 hours in transfer buffer containing 119 mM Tris (pH 8.5), 40 mM glycine, 0.1% SDS, and 20% Methanol. Membranes were blocked with 5 % skimmed milk in PBS (154 mM NaCl, 1.5 mM KH_2PO_4, 5.5 mM Na_2HPO_4) for 30 minutes, then incubated with relevant primary antibodies recognizing α-tubulin (1:2000, DM1A, Sigma-Aldrich; as a loading control), SMC2 (1:1000) (17), or GFP (1:1000) (gift from Simona Saccani, University of Edinburgh) with 1% skimmed milk in PBS/tween20 (1%) for 3 hours up to overnight. Membranes were washed three times for 5 minutes with PBS/tween20 (1%). Membranes were incubated with IRDye-labeled secondary antibodies diluted in 1% skimmed milk in PBS/tween20 (1%) (1:10,000) for 45 minutes followed by three 5 minute washes with PBS/tween20 (1%). Membranes were kept in PBS until fluorescence intensities were determined

using a CCD scanner (Odyssey; LI-COR Biosciences) according to the manufacturer's instructions.

Flow cytometry analysis

DNA content: Cells were suspended overnight in ice-cold 70% ethanol. The next morning, cells were rinsed with PBS then re-suspended in PBS containing 100 µg/ml RNase A and 5 µg/ml propidium iodide. Samples were then analyzed using a FACSCalibur flow cytometer following the manufacturer's instructions. Data was analyzed using FlowJo V10.3. WT cells were gated for viability based on forward and side scatter (FSC/SSC), from which single cells were selected based on FSC height (H) and width (W). These gates were applied to all samples and DNA content was plotted as a histogram of FSC-H.

Chromatin Enrichment for Proteomics (ChEP)

Synchronized Cdk1as cells were crosslinked with 1% formaldehyde at specified time points in mitosis and chromatin was extracted from the crosslinked cells by the ChEP protocol (*55*). Briefly, 5 x 10^7 cells were fixed for 10 minutes by addition of formaldehyde to the cell culture. Formaldehyde was quenched by 125 mM glycine for 5 minutes. Crosslinked cells were washed with TBS (20 mM Tris pH 7.4, 150 mM NaCl) and frozen in liquid nitrogen. Cells were lysed on ice in Lysis buffer (25 mM Tris pH 7.4, 0.1% Triton X-100, 85 mM KCl, protease inhibitors: 1 mM PMSF, 1 µg/ ml each of chymostatin, leupeptin, antipain, pepstatin A). Cells were washed with Lysis buffer and the pellet was resuspended in 300 µl SDS buffer (50 mM Tris pH 7.4, 10 mM EDTA, 4% SDS, protease inhibitors as above) for 10 minutes at room temperature. Next, 3 volumes of Urea buffer (10 mM Tris pH 7.4, 1 mM EDTA, 8M Urea) were added and samples centrifuged at 16,000 x *g* for 30 minutes. The pellet was again resuspended in 1 volume of SDS buffer, then 3 volumes of Urea buffer was added before centrifugation again. The pellet was washed with SDS buffer before resuspension in ice cold storage buffer (10 mM Tris pH 7.4, 1 mM EDTA, 25 mM NaCl, 10% glycerol). Chromatin DNA was sheared by sonication. The solubilized chromatin was mixed with 3x SDS sample buffer (6% SDS, 150 mM Tris pH 6.8, 30% glycerol) and heated at 95°C for 30 minutes to reverse the crosslinks. 10% of the sample

was electrophoresed in a NuPAGE Bis-Tris gel (NP0335, Invitrogen). The de-crosslinked chromatin proteins were in-gel digested with 2µg trypsin overnight (> 16hours). The tryptic peptides were analyzed by liquid chromatography coupled with tandem mass spectrometry (LC-MS/MS). Data was analyzed with MaxQuant 1.5.7.4 (*81*). The abundance of proteins was estimated using the iBAQ algorithm (*82*), and normalized by the copy number of histone H4 (*83*).

Hi-C protocol

Chromosome conformation capture was performed as described previously (*84*). Briefly, 10-20x10^6 cells were cross-linked in 1% formaldehyde for 10 minutes and quenched in 125 mM glycine. Cells were snap-frozen and stored at -80°C before cell lysis.

Cells were lysed for 15 minutes in ice cold lysis buffer (10 mM Tris-HCl pH8.0, 10 mM NaCl, 0.2% Igepal CA-630) in the presence of Halt protease inhibitors (Thermo Fisher, 78429) and cells were disrupted by homogenization with pestle A for 2x 30 strokes. Chromatin was solubilized in 0.1% SDS at 65°C for 10 minutes, quenched by 1% Triton X-100 (Sigma, 93443) and chromatin was digested with 400 units of HindIII (NEB, R0104) overnight at 37°C.

Fill-in of digested overhangs by DNA polymerase I, large Klenow fragment (NEB, M0210) in the presence of 250 nM biotin-14-dCTP (Life Technologies, 19518-018) for a minimum of 90 minutes was performed prior to 1% SDS based enzyme inactivation and dilute ligation with T4 DNA ligase (Life Technologies, 15224) for 4 hours at 16°C. Cross-links of ligated chromatin were reversed overnight by proteinase K (Life Technologies, 25530-031) incubation at 65°C. DNA was isolated with 1:1 phenol:chloroform, followed by 30 minutes of RNase A incubation.

Biotin was removed from unligated ends by incubation with 15 units of T4 DNA polymerase in the presence of 25 nM dATP/dGTP. DNA was sheared using an E220 evolution sonicator (Covaris) and size selected with Agencourt AMPure® XP (Beckman Coulter) to 150-350 bps. After end repair in a mixture of T4 polynucleotide kinase (25 units; NEB, M0201), T4 DNA polymerase (7.5 units; NEB, M0203L) and DNA polymerase I, large (Klenow) fragment

(2.5 units; NEB, M0210) at 20°C for 30 minutes, dATP was added to blunted ends using 15 units of polymerase I, large fragment (Klenow 3' → 5' exo-) (NEB, M0212L) at 37°C for 30 minutes.

Biotinylated DNA was collected by incubation in the presence of 10 µl of streptavidin coated myOne C1 beads (Life technologies, 650.01) and Illumina paired-end adapters were added by ligation with T4 DNA ligase (Life technologies) for 2 hours at room temperature. A PCR titration (primers PE1.0 and PE2.0) was performed prior to a production PCR to determine the minimal number of PCR cycles needed to generate a Hi-C library. Primers were separated from the library using Ampure size selection prior to 50 bp paired-end sequencing on an Illumina HiSeq sequencer (Life Technologies).

Hi-C data analysis

Briefly, we processed Hi-C data as described in (33), with multiple modifications, including using the galGal5 genome assembly. All scripts mentioned below to be from the Dekker Lab c-world pipeline are available at a GitHub repository (*85*). cMapping at https://github.com/dekkerlab/cMapping; iterative correction (balancing) at https://github.com/dekkerlab/balance and analysis scripts at https://github.com/dekkerlab/cworld-dekker. The Mirny Lab software, including the *cooler* library for storage and analysis of Hi-C data is available at https://github.com/mirnylab.

Mapping sequenced Hi-C reads

Fastq files were mapped and binned using the c-world mapping pipeline. Briefly, 50 bp paired end reads obtained as fastq files were truncated to 25 bp starting at the 5' end. Then, they were iteratively mapped (*86*) to the Red Jungle Fowl laboratory line chicken genome (UCSC Genome Browser assembly ID: galGal5, Dec. 2015, Accession ID: GCF_000002315.4; NCBI genome/111 (Gallus gallus)(*87*). Uniquely mapped, paired reads were kept and assigned to a HindIII restriction fragment assigned through its 5' position. Mapped reads were filtered for same fragment ends and uniqueness, excluding PCR duplicates (defined as sequence matches with the exact same start and end).

P(s) curves.

We used the mapped reads to calculate the functions of contact frequency P(s) vs genomic separation s. We split all genomic distances between 1 kb and 1Gb into bins of exponentially increasing widths, such that the upper edge of every bin was 1.12 larger than the lower edge. For every such separation bin, we found the number of observed *cis*-interactions within this range of separations and divided it by the number of all loci pairs, separated by such distances *in cis*.

Binning and balancing of Hi-C data

Unique valid pair reads were binned to 50 and 100 kb bins, using cooler package, and noisy or low signal bins were excluded prior to balancing using the MADmax filter: we removed all bins, whose coverage was 7.4 genome-wide median deviations below the median bin coverage. Matrices were balanced by iterative correction (IC), equalizing the sum of every row/column to 1.0 (*88*), using *cooler (https://github.com/mirnylab/cooler).*

Compartment analysis

Compartments were quantified using principal component analysis on 100 kb binned data using the *matrix2compartment* perl script in our c-world pipeline. The largest eigenvector (eig1) typically represents the compartment profile (*3*, *30*, *89*). When compartment signals were low or absent, we checked consecutive eigenvectors to confirm loss of compartments. We also plotted the cumulative explained variance for the first 10 eigenvectors (**Fig. S3, S17**). Per convention A/B-compartments were assigned by gene density, so that the A-compartment was more gene-dense than the B-compartment.

In order to measure the strength of compartmentalization, we used the observed/expected Hi-C maps, which we calculated from 100 kb iteratively corrected interaction maps of cis-interactions by dividing each diagonal of a matrix by its chromosome-wide average value. In each observed/expected map, we rearranged the rows and the columns in the order of increasing eigenvector value. Finally, we aggregated the rows and the columns of the resulting matrix into 30 equally sized aggregated bins, thus obtaining a compartmentalization plot (or, a saddle plot).

Insulation analysis (TADs)

TAD calling was performed on 50 kb binned data exactly as described previously (30). We first determined the optimal insulation square for TAD calling with our c-world pipeline perl script *matrix2insulationRange*. We used a range of insulation squares from 50 kbp (*istart* variable) to 1 Mb (*iend* variable) with a 50 kb (bin size) step (*istep* variable) to sweep through the insulation topology. From this sweep, we determined to use a 250x250 kb sliding square (*is* = 250000) along the matrix diagonal without smoothing (*ss* = 50000) for capturing the aggregate TAD signal for galGal5 (**Fig. S5**). For 40 kb binned HelaS3 (ATCC CCL2.2) Hi-C data, we detected TADs using a 520x520 kb sliding square (*is* = 520000) without smoothing (*ss* = 40000). These settings were used as input variables for insulation square analysis with the *matrix2insulation* perl script from our c-world pipeline. Briefly, the inter quartile (IQR) mean signal within the square (*im* = iqrMean) was assigned to the diagonal bin and this process was repeated for all bins. The insulation score was then normalized relative to average score of the insulation scores across each chromosome by calculating the log2 ratio of each bin's insulation score and the mean of all insulation scores, as described previously (30). Minima along the normalized insulation score vector represent loci of high local insulation and are interpreted as TAD boundaries. For aggregate insulation score pileups, bed files with TAD boundary positions from G_2 arrested cells were used as input for each mutant cell line separately (*ebf* variable). TAD boundary pileups were generated for 50 kb steps (*mindist* = 50000) covering 500 kb upstream and 500 kb downstream from TAD boundaries (ezs = 500000) with a maximum interaction distance of 500 kb (*maxdist* = 500000) using our *elementPileUp* c-world perl script.

Coarse-grained model of contact probability decay in mitotic chromosomes

In the coarse-grained model loops are regularly placed along the axis of the chromosome (z-axis) with a spacing Δ_z. Each loop is represented by a cylindrical wedge, where loci that belong to this loop are distributed normally along the z directions, with mean at the base of the loop and the standard deviation σ), and normally in the angular position with the mean at the orientation of the loop and the standard deviation φ. Orientation of each loop depends on the model and can be uniformly random (*Randomly oriented uncorrelated loops*), correlated with its neighboring loops, forming an angular random walk (*Loops with correlated orientation*), or form a random walk while having a preferred orientation (*Loops with spiral staircase orientation*).

Below, we derive an approximate expression for the probability of a contact between two loci $P_c(s)$, separated by genomic distance s, in a chromosome compacted into an array of consecutive loops. Naturally, this expression has two regimes: (a) the intra-loop regime at shorter genomic separations, where the two loci are located on the same loop, and (b) the between-loop regime at larger separations, when loci are located on different loops. If the lengths of loops are random and distributed exponentially, the transition between the regimes occurs around the genomic separation comparable to the average loop length l_{avg}:

$$P_c(s) = e^{-s/l_{avg}} P_c^{in}(s) + \left(1 - e^{-s/l_{avg}}\right) P_c^{between}(s) \qquad (1)$$

Contacts within loops

The simplest model of individual loop conformations is a random walk in 3D. In this case, the contact probability decays as a power-law with a -3/2 exponent, assuming poor solvent conditions in the melt of loops, and neglecting correction for the closed loop:

$$P_c^{in}(s) = C_{in}\, s^{-1.5} \qquad (2)$$

This scaling is consistent with $P_c(s)$ observed even at larger distances during interphase in very large oocyte nuclei (*90*). Below, we will not attempt to improve this simple model, and instead focus on long-distance behavior of $P_c(s)$, which reflects the mutual arrangement of loops.

Contacts between loops

By definition, a contact between two loci occurs when they have similar coordinates, either in Cartesian or cylindrical coordinates:

$$P_c^{between}(s) = C_{between}P\left(x_i = x_j, y_i = y_j, z_i = z_j\right) = C_{between}P\left(r_i = r_j, \theta_i = \theta_j, z_i = z_j\right)$$

For two loci located on different loops, we can simplify this expression drastically by assuming that the probabilities of overlap at each coordinate are independent of each other:

$$P_c^{between}(s) = C_{between}P\left(r_i = r_j\right)P(\theta_i = \theta_j)\ P(z_i = z_j) \qquad (3)$$

Randomly oriented uncorrelated loops

In order to estimate the probability of contact between loci on different loops, we have to make extra assumptions on the mutual orientations of these loops. In the simplest case, each loop is randomly oriented and the orientations of consecutive loops are not correlated with each other. In this case, both $P_c\left(r_i = r_j\right)$ and $P_c\left(\theta_i = \theta_j\right)$ are independent of the separation between the loops and thus integrate to a constant, leaving:

$$P_c^{uncorr}(s) = C_{between}P\left(z_i = z_j\right) = C_{between}P_c^z(s)$$

We can calculate this remaining expression easily if we assume that the loci within each loop are normally distributed along the z-axis, each around the base of its loop:

$$P_c^z(s) = C\int_{-\infty}^{\infty}\int_{-\infty}^{\infty} N(z_i, \overline{z_i}, \sigma)N\left(z_j, \overline{z_j}, \sigma\right)\delta\left(z_i - z_j\right)dz_i dz_j$$

In this expression, N(x, mean, s.d.) is the PDF of the normal distribution, i and j are the genomic coordinates of the two loci, z_i and z_j are the axial coordinates in the 3D genomic structure, $\overline{z_i}$ and $\overline{z_j}$ are the expected axial coordinates of the i-th and j-th loci (which, by our assumption, are equal to the axial coordinates of their corresponding loop bases), σ is the measure of the spread of loop

along the axis of the chromosome, i.e. the high of each loop, and $\delta(z_i - z_j)$ is the delta function that limits the integral only to the conformations where the particles have the same axial coordinate. Taking this integral gives us:

$$P_c^z(s) = C\ N(\bar{z_i} - \bar{z_j}, 0, \sqrt{2}\sigma)$$

Finally, if the loops are regularly places along the axis of the chromosome with a spacing Δ_z, than the expected axial distance between the bases of two loops is equal the expected number of loops between these two loci, multiplied by Δ_z:

$$P_c^z(s, l_{avg}, \Delta_z, \sigma)(s|\ l_{avg}, \Delta_z, \sigma) = C\ N\left(\Delta_z \frac{s}{l_{avg}}, 0, \sqrt{2}\sigma\right) = C'\ N\left(\frac{s}{l_{avg}}, 0, \frac{\sqrt{2}\sigma}{\Delta_z}\right) \quad (4)$$

$P_c^Z(s)$ describes the decay of contact probability due to the decreasing axial overlap of more distant loops and, as illustrated in **Fig. 1B**, produces a characteristic drop-off in log-log representation of $P_c(s)$. The drop takes place at when the number of loop s/l_{avr} exceeds ~$2\sqrt{2}\sigma$ /Δ_z the ratio of the loop high and the separation between loop.

For example, at prophase a drop at 4.5Mb for loops of the average size l_{avr} = 80Kb requires 56 loops per layer. Hence $2\sqrt{2}\sigma$ /Δ_z = 56; then for σ= 200nm of loop high, one gets Δ_z=7.5nm separation between neighboring loops. This is a tight packing at the scaffold, but feasible with 10nm fiber emanating from condensins, possibly requiring the scaffold to wiggle inside the chromosome. For prometaphase, a drop at 10Mb and 80Kb loops leads to 125 loops per layer, and the spacing of 3nm, which is smaller than protein domains of condensin, necessitating nested loops and considerable winding of the scaffold inside the chromosome.

Loops with correlated orientation

$P_c^z(s)$ alone does not fully explain the experimentally observed $P_c(s)$ curves: it explains the origin of a drop in contact probability at longer distances, but does not explain the origin of a gradual decay before the drop. Equation (3) then suggests that this extra gradual decay might be due to the angular overlap $P(\theta_i = \theta_j)$. Specifically, if the angular orientations of consecutive loops are somehow correlated, forming the angular (1D) random walk, this would increase the frequency

of angular overlaps for loci in adjacent loops and make it smaller for loci that are contained in distant loops.

$$P_c^{corr}(s) = C_{between} P(z_i = z_j) P(\theta_i = \theta_j) = C_{between} P_c^z(s) P_c^{ang,corr}(s) \quad (5)$$

We can derive the frequency of angular overlaps explicitly:

$$P_c^{ang,corr}(s) = \int_{-\infty}^{\infty}\int_{-\infty}^{\infty}\int_{-\infty}^{\infty} N(\theta_i, 0, \phi) N(\theta_j, \bar{\theta}_j, \phi) N\left(\bar{\theta}_j, 0, \gamma\sqrt{s/l_{avg}}\right) \sum_{k=-\infty}^{\infty} \delta(\theta_i - \theta_j + 2\pi k)\, d\theta_i d\theta_j d\bar{\theta}_j$$

Here, θ_i and θ_j are the angular coordinates of the two loci, which are distributed normally around the mean angular orientation of their loops (0 and $\bar{\theta}_j$, correspondingly) with the standard deviation φ. The correlations in the orientations of adjacent loops lead to the fact that the mean angular orientation of the loop with the j-th locus, $\bar{\theta}_j$, is normally distributed itself around the mean of 0 (which we picked to be the angular orientation of the loop with the i-th locus, without a loss of generality) and the standard deviation of $\gamma\sqrt{s/l_{avg}}$. The latter is calculated from the assumption the angles of two consecutive loops on average differ by γ; thus, between the i-th and j-th locus there are s/l_{avg} loops, each taking a random step of γ, thus producing a 1D random walk with the standard deviation of $\gamma\sqrt{s/l_{avg}}$. Taking all integrals gives us:

$$P_c^{ang,corr}(s) = \int_{-\infty}^{\infty} \sum_{k=-\infty}^{\infty} N(\bar{\theta}_j + 2\pi k, 0, \sqrt{2}\phi)\, N\left(\bar{\theta}_j, 0, \gamma\sqrt{s/l_{avg}}\right) d\bar{\theta}_j$$

$$P_c^{ang,corr}(s, l_{avg}, \phi, \gamma)(s|\, l_{avg}, \phi, \gamma) = C\left(\gamma^2 \frac{s}{l_{avg}} + 2\phi^2\right)^{-0.5} \quad (6)$$

$P_c^{ang,corr}$ describes the decay of contact probability with distance due to gradually decaying correlations of more distant loops. For a range of parameters, it can produce a characteristic -0.5 power-law decay of $P_c(s)$, before the random walk fills the whole 2π In combination with the drop-off decay due to decreasing axial co-localization, P_c^z, these two terms produce a prophase-like three-regime decay of contact probability, as illustrated in **Fig. 1B**.

Interestingly, when the angular random walk fills a full circle the angular part of the contact probability becomes constant and independent of *s*, i.e. $P_c^{ang\ corr}(s) \sim s^{-0.5}$, while the angular displacement $\gamma\sqrt{s/l_{avg}} < 2\pi$. For more loops per layer $P_c(s)$=const is expected to appear. Since we don't see this regime in the data, it means that $\sqrt{s/l_{avg}} < 2\pi$ for s within a layer. Hence for a drop at 10Mb and 80Kb loops, we get 125 loops per layer and $\gamma < 2\pi/11$, so the angle between loops should be below or around 30 degrees.

Loops with spiral staircase orientation

Finally, we build a model that could explain the non-monotonic dependency of contact probability with separation, observed in Hi-C of prometaphase chromosomes. This non-monotonicity could be explained by spiralization of chromosomes, previously observed with an electron microscope. In our model, we can describe this spiralization as periodicity of the angular orientations of loops. In order to agree with the experimental data, we have, however, to combine this periodicity at larger scales with random correlated angular loop orientations at shorter separations.

These properties could all be achieved when the angular orientations of loops follow a 1D random walk under the constraint that each loop cannot deviate too much from its preferred orientation, set by the spiral, i.e., linearly proportional to its index. The probability of an angular overlap between loci on two loops can be calculated as the probability of a return of such 1D random walk to its initial position after s/l_avg steps. These random walks are known under the name of the Ornstein-Uhlenbeck (OU) processes, and their properties, including the return probability, have been studied in the theory of stochastic processes (*91*):

$$P_c^{OU}(s) = C_{between} P(z_i = z_j) P(\theta_i = \theta_j) = C_{between} P_c^z(s) P_c^{ang,OU}(s)$$

$$P_c^{ang,OU}(s) = \sum_{k=-\infty}^{\infty} N\left(2\pi k, \Delta_\theta s/l_{avg}, \sqrt{2\phi^2 + \gamma^2 n_{return}(1 - e^{s/l_{avg}/n_{return}})}\right)$$

Here, Δ_θ is the systematic shift of the angle per loop (which produces the spiral phenotype). n_{return} is the parameter of the Ornstein-Uhlenbeck process characterizing the variability of the angular loop orientations around their optimal orientation: the loops deviate on average by $\sqrt{n_{return}}\gamma$ from their optimal angular orientation and the n_{return} consecutive loops have correlated orientations. We also modified the standard formula for the return probability of the trending OU process to account for the fact that, in angular coordinates, two points overlap when they have the same angle modulo 2*pi.

Bridging the in-loop and between-loop regimes

Note that both expressions of P_c^{in} and $P_c^{between}$ contain arbitrarily defined coefficients C_{in} and $C_{between}$. In order to obtain a unified expression that describes the contact probability at all length scales, we need adjust these coefficients, such that $P_c^{in}(s)$ and $P_c^{between}$ could be directly compared to each other. Both of these coefficients are arbitrary and their ratio only affects the narrow transitional region at s ~ 1-3 l_{avg}. In the calculations presented in the paper, we calculate these coefficients by matching the two curves at the separation of two average loop sizes:

$$P_c^{in}\left(\frac{2s}{l_{avg}}\right) = P_c^{between}\left(\frac{2s}{l_{avg}}\right)$$

Polymer models of mitotic chromosomes

The design of Langevin molecular dynamics simulations of chromosomes

In order to test the proposed architectures of prophase and prometaphase chromosomes against our Hi-C data, we simulate polymer models of chromosomes using Langevin molecular dynamics. The overall design of these simulations is similar to that in (8, 23), with a few major differences. We model 10nm 'beads-on-string' chromatin fiber of nucleosomes as a chain of 10nm particles, each representing one nucleosome with 200bp of DNA. These particles are connected by springs with a using a harmonic potential with an equilibrium length of 10nm and

the stiffness coefficient of 1 kbT/nm^2. We simulated repulsion between spatially overlapping nucleosomes using the following force potential:

$$U = 5\left(-1+\left(\frac{0.105\cdot r}{\sqrt{6/7}}\right)^{12}\cdot\left(\left(\frac{0.105\cdot r}{\sqrt{6/7}}\right)^{2}-1\right)\cdot\frac{823543}{46656}\right)k_bT$$

This potential is designed to be constant of 5.0 kbT until r = 7-8nm, and then rapidly go to zero around 10.5 nm. The limited maximum overlap energy of 5.0 kbT allowed chromatin fibers to pass through each other occasionally and thus accounted for the strand-passing activity topoisomerase II. In all of our simulations, we additionally compact chromosomes using cylindrical constraints to impose the high chromatin density of one nucleosome per 11nm x 11nm x 11nm box, as observed in EM images of mitotic chromosomes. The particular geometric parameters of the cylindrical constraint varied between simulations. We imposed this constraint using a harmonically increasing potential with k=0.1 kbT when monomer crossed the boundaries of the constraining cylinder. We perform Langevin dynamics polymer simulations using OpenMM, a high-performance GPU assisted molecular dynamics API (*92*, *93*). We used the following parameters of the Langevin dynamics – variable time step to achieve the relative accuracy of 0.001, the friction coefficient of 0.01, particle mass of 1.0 and the temperature of 300K. We ran the simulations until the simulated *P(s)* curves (see below) stopped changing at logarithmic time scales, which occurred after 1.5e7 timesteps in prophase simulations and after 3e6 timesteps in prometaphase simulations. We visualized the resulting chromosome structures using Pymol (DeLano, Warren Lyford. "PyMOL." (2002)).

Simulations of prophase and CAP-H2-depleted chromosomes

We simulated prophase chromosomes as arrays of consecutive loops compacted into a cylindrical shape with a high chromatin density. As in (8), we first randomly selected a subset of particles to be bases of consecutive loops, such that the loop lengths were exponentially distributed with an average of l_{avg}. We modelled loop-forming condensins by imposing extra harmonic bonds between the particles representing loop bases. Finally, we tethered the first and

the last particles of the chromosome to the ends of the compacting cylinder using a harmonic attraction potential along z-coordinate with k=0.15 kbT/nm^2. We equilibrated the each simulation for 1.5e7 steps to allow for slow large-scale rearrangement of the flexible chromosome scaffold. To match the simulations with the WT prophase and CAPH2 prometaphase experiments, we systematically varied the two model parameters: (1) the average loop length, l_{avg}, from 20 kb and 100 kb, with a step of 10 kb and (2) the average linear density of loops along the axis of the constraining cylinder, N_{loops}/L, from 50 loops/μm to 350 loops/μm, with a step of 50 loops/μm. For each parameter set, we modeled a chromosome containing 500 average loop lengths.

Simulations of prometaphase and CAP-H-depleted chromosomes

We simulated prometaphase chromosomes as helical arrays of consecutive nested loops compacted into a cylindrical shape with a high chromatin density. As in the prophase simulations above, we first imposed an array of consecutive loops with the average loop length of l_{avg}^{outer}. To account for the action of condensin I, we further split each of these "outer" loops into an array of smaller exponentially distributed "inner" loops, with an average length l_{avg}^{inner}. To test if the Hi-C data is consistent with helical winding of prometaphase chromosomes, we fixed the bases of the "outer" loops along a 3-dimensional helical path winding around the axis of the constraining cylinder. We imposed this helical path by tethering each loop base to its specific position along the helix with a harmonic potential with k=0.04 kbT/nm^2. We equilibrated each simulation only for 1e6 steps, since the motion of the backbone was suppressed and only individual loops had to equilibrate. To match the simulations with the prometaphase experiments, we varied four parameters of the model: (1) the average inner loop size, l_{avg}^{inner}, from 20 kb to 100 kb every 20 kb; (2) the average outer loop size l_{avg}^{outer} as a multiple of the average inner loop size l_{avg}^{inner}, from 1 to 11 inner loops, with a step of 2; (3) the average amount of DNA per helical turn, P, from 2 to 15 Mb, with a step of 1 Mb; (4) the pitch of the helical scaffold, b, from 50 to 300nm, with a step of 50nm. As above, for each parameter set, we modeled a chromosome containing 500 l_{avg}^{outer}. For each parameter set, the length of the constraining cylinder matched the axial length of the helical scaffold, and the radius of the cylinder was adjusted to reach the density of 1 particle per 11nm x 11 nm x 11 nm box.

Simulated Hi-C and P(s) calculation for polymer models

We then used our polymer models to perform in-silico Hi-C. For each polymer model, we picked the chromosome structure at the end of the simulation and found all pairs of contacting monomers, i.e. pairs of monomers separated by less than 51nm in 3D space. As in the experimental Hi-C, we used these pairs to calculate the contact frequency vs separation *P(s)* curves.

Model selection via comparison of simulated and experimental P(s) curves

To find which simulations produce the best agreement with the experimental data, we systematically tried all possible combination of the model parameters. For each parameter set, we performed a simulation, generated a *P(s)* curve and calculat the root mean square (r.m.s.) difference with the experimental *P(s)* in the log10-log10 scale, after normalizing both of the curves at the specific distance (see the table below). Our simulations cannot predict *P(s)* both at very short separations, below a loop size, and at very long separations, after the drop-off; for that reason, we limit our *P(s)* discrepancy computations to ranges shown in the table below. Finally, we equalize the contribution of the short- and long-distance parts of the *P(s)* (see the table below) by calculating the r.m.s. *P(s)* difference in each of these regions separately and reporting the mean of the two.

Experiment	The short-distance region of *P(s)*	The long-distance region of *P(s)*	The genomic distance of normalization, bp
WT-2m	20 kb-200 kb	200 kb-1 Mb	100 kb
WT-5m	20 kb-200 kb	200 kb-2 Mb	100 kb
WT-7m	20 kb-200 kb	200 kb-4 Mb	100 kb
WT-10m	20 kb-200 kb	200 kb-4 Mb	100 kb
WT-15m	100 kb-1 Mb	1 Mb-15 Mb	100 kb
WT-30m	100 kb-1 Mb	1 Mb-15 Mb	100 kb

WT-60m	100 kb-1 Mb	1 Mb-20 Mb	100 kb
CAPH2-7m	20 kb-200 kb	200 kb-1 Mb	100 kb
CAPH2-10m	20 kb-200 kb	200 kb-2 Mb	100 kb
CAPH2-15m	20 kb-200 kb	200 kb-2 Mb	100 kb
CAPH2-30m	20 kb-200 kb	200 kb-3 Mb	100 kb
CAPH2-60m	20 kb-200 kb	200 kb-3 Mb	100 kb
CAPH1-15m	300 kb-3 Mb	3 Mb-10 Mb	300 kb
CAPH1-30m	300 kb-3 Mb	3 Mb-20 Mb	300 kb
CAPH1-60m	300 kb-3 Mb	3 Mb-40 Mb	300 kb

P(s) estimation for prophase models with sister chromatid cohesion

In order to understand how the presence of a spatially proximal sister chromatid could change the *P(s)* curves we performed a mock-up simulation. We considered the 3D structure of the best-fitting prophase model and added to it its identical copy shifted along the direction perpendicular to the chromatid axis by distance Δ_x^{sister}. We then calculated the *P(s)* for this structure, under the assumption that our *in-silico* Hi-C procedure could not tell apart the corresponding identical loci on the two chromatids. We then repeated this procedure for different values of Δ_x^{sister}, from 0 (a complete overlap between the two chromatids) to 2 chromatid radii (a complete segregation of the chromatids).